2018

An Overview of Anorthosite-bearing Layered Intrusions in the Archaean Craton of Southern West Greenland and the Superior Province of Canada: Implications for Archaean Tectonics and the Origin of Megacrystic Plagioclase

Ali Polat
University of Windsor

Fred J. Longstaffe
The University of Western Ontario, flongsta@uwo.ca

Robert Frei
University of Copenhagen

An overview of anorthosite-bearing layered intrusions in the Archaean Craton of southern West Greenland and the Superior Province of Canada: Implications for Archaean tectonics and the origin of megacrystic plagioclase

Ali Polat

Department of Earth and Environmental Sciences, University of Windsor, Windsor, Canada

Fred J. Longstaffe

Department of Earth Sciences, The University of Western Ontario, London, Canada

Robert Frei

Department of Geoscience and Natural Resource Management, University of Copenhagen, København, Denmark

Corresponding author: Ali Polat (polat@uwindsor.ca)

An overview of anorthosite-bearing layered intrusions in the Archaean Craton of southern West Greenland and the Superior Province of Canada: Implications for Archaean tectonics and the origin of megacrystic plagioclase

ABSTRACT

Anorthosite-bearing layered intrusions are unique to the Archaean rock record and are abundant in the Archaean craton of southern West Greenland and the Superior Province of Canada. These layered intrusions consist mainly of ultramafic rocks, gabbros, leucogabbros and anorthosites, and typically contain high-Ca (>An_{70}) megacrystic (2-30 cm in diameter) plagioclase in anorthosite and leucogabbro units. They are spatially and temporally associated with basalt-dominated greenstone belts and are intruded by syn-to post-tectonic granitoid rocks. The layered intrusions, greenstone belts and granitoids all share the geochemical characteristics of Phanerozoic subduction zone magmas, suggesting that they formed mainly in a suprasubduction zone setting. Archaean anorthosite-bearing layered intrusions and spatially associated greenstone belts are interpreted to be fragments of oceanic crust, representing dismembered subduction-related ophiolites. We suggest that large degrees of partial melting (25-35%) in the hotter (1500-1600°C) Archaean upper mantle beneath rifting arcs and backarc basins produced shallow, kilometre-scale hydrous magma chambers. Field observations suggest that megacrystic anorthosites were generated at the top of the magma chambers, or in sills, dykes and pods in the oceanic crust. The absence of high-Ca megacrystic anorthosites in post-Archaean layered intrusions and oceanic crust reflects the decline of mantle temperatures resulting from secular cooling of the Earth.

Keywords: word; Archaean layered intrusion, megacrystic anorthosite, leucogabbro, magma chamber, suprasubduction zone

1. Introduction

Although they are volumetrically small, Archaean anorthosite-bearing layered intrusions are widespread both in western Greenland and the Superior Province of Canada (Windley, Herd, & Bowden, 1973; Myers, 1985; Daigneault, ST-Julien, & Allard, 1990; Ashwal, 1993, 2010; Owens & Dymek, 1997; Peck, Messing, Halden, &

Chandler, 1998; Dymek & Owens, 2001; Gilbert 2007; Windley & Garde, 2009; Hoffmann, Svahnberg, Piazolo, Scherstén, & Münker, 2012; Percival et al. 2012; Zhou et al., 2016; Ashwal & Bybee, 2017). Anorthosites are also a ubiquitous component of Proterozoic orogenic belts and Phanerozoic ophiolites (Table 1), and have been recovered from modern oceanic crust (Ashwal, 2010). Archaean anorthosites are distinct from Proterozoic and Phanerozoic counterparts in that they commonly contain equidimensional, rounded high-Ca (An_{70-93}) plagioclase ranging from 2 to 30 cm in diameter, and are associated with layers of leucogabbro, gabbro, and ultramafic rocks (Myers, 1985; Ashwal, 1993; Peck, Messing, Halden, & Chandler, 1998; Polat et al., 2009; Ashwal & Bybee, 2017). These layered intrusions are typically associated with tholeiitic to calc-alkaline basalt-dominated volcanic rocks in greenstone belts, and are intruded mainly by syn- to post-tectonic tonalite-trondhjemite-granodiorite suites (TTGs) (Davis, Sutcliffe, & Trowell, 1988; Daigneault, ST-Julien, & Allard, 1990; Leclerc et al., 2011; Zhou et al., 2016; Polat, Wang, & Appel, 2015).

Despite their widespread occurrence, Archaean megacrystic anorthosites are among the least understood rock types in the Earth's crust (Phinney, Donald, & David, 1988; Ashwal, 1993, 2010; Ashwal & Bybee, 2017). Several outstanding petrogenetic and geodynamic questions remain to be revolved to constrain their origin. These questions include: (1) How did anorthosites originate in the first place? (2) How were they emplaced into the crust? (3) What type of crust (oceanic versus continental) did they intrude? (4) Why do they have plagioclase crystals up to 30 cm in diameter? (5) What was the geodynamic setting(s) that produced these rocks? (6) Why are they rare in post-Archaean times?

In this contribution, we use the geological and geochemical characteristics of well-studied Mesoarchaean to Neoarchaean anorthosite-bearing layered intrusions in western Greenland (Ivisaartoq, Fiskenæsset, Naajat Kuuat complexes) and the Superior Province of Canada (Bad Vermilion Lake and Doré Lake complexes) to address the above questions and propose a new geodynamic model for the petrogenetic origin of these rocks (Figs. 1, 2). Emphasis is placed on the megacrystic anorthosites and leucogabbros in the Fiskenæsset Complex where most stages of anorthosite and leucogabbro development are well exposed (Figs. 3, 4). In addition, we present new major and trace element and petrographic data from the Sinarssuk area in the Fiskenæsset region to provide new constraints on the origin of megacrystic anorthosite and leucogabbros. Analytical methods of major and trace elements for the new analyses are the same as described in Polat et al. (2011). The method used for Scanning Electron Microscope–Energy Dispersive Spectroscopy (SEM–EDS) analyses is given in Price (2012).

2. Regional geology

2.1. Archean craton of southern West Greenland

The Archaean terrain of West Greenland is composed of Eoarchaean to Neoarchaean tectonically-accreted crustal blocks, consisting predominantly of TTG and granitic gneisses, basalt-dominated greenstone belts (volcanic and sedimentary rock associations), anorthosite-bearing layered intrusions, and granites (Friend & Nutman, 2005; Steenfelt, Garde, Moyen, 2005; Windley & Garde, 2009; Polat, Wang, & Appel, 2015). The poly-deformed and metamorphosed greenstone belts and anorthosite-bearing layered intrusions occur as meter- to kilometer-scale conformable layers within the TTG gneisses. Contacts between the TTG gneisses and greenstone belts and anorthosite-bearing layered intrusions are characterized predominantly by 5 to 20 meter wide mylonitic shear zones with rare intrusive relationships (Windley & Garde, 2009; Polat, Wang, & Appel, 2015). The anorthosite-bearing layered intrusions are commonly spatially associated with volcanic rocks and are interpreted to have been emplaced into oceanic basaltic to gabbroic rocks, and they are in turn intruded by syn-tectonic TTGs (Myers, 1976; Windley & Garde, 2009; Hoffmann, Svahnberg, Piazolo, Scherstén, & Münker, 2012). The greenstone belts consist of tholeiitic to calc-alkaline basalts, boninites and picrites with minor siliciclastic sedimentary rocks. The anorthosite-bearing layered intrusions are composed mainly of cumulate layers of anorthosite, leucogabbro, gabbro and ultramafic rocks (Fig. 4). Field, geochronological and geochemical investigations suggest that the Archaean craton of southern West Greenland grew at convergent plate margins through accretion of island arcs and continental blocks (Nutman, Friend, & Bennett, 2002; Friend & Nutman, 2005; Garde, 2007; Windley & Garde, 2009; Kisters, van Hinsberg, & Szilas, K., 2012; Szilas et al., 2012; Szilas et al., 2013; Dziggel, Diener, Kolb, & Kokfelt, 2014; Polat, Wang, & Appel, 2015). Despite poly-phase deformation and amphibolite to granulite facies metamorphism, primary structures (e.g., pillows) in the volcanic rocks and cumulate textures and igneous layering in the anorthosite-bearing layered intrusions are well preserved (Chadwick, 1985, 1990; Myers, 2001; Windley & Garde, 2009; Polat et al., 2008; Polat et al., 2011; Polat, Wang, & Appel, 2015).

Windley and Garde (2009) divide the Archaean craton of southern West Greenland into six Mesoarchaean to Neoarchaean (ca. 3000–2720 Ma) tectonic blocks that display similar geological cross-sections (Fig. 1). These blocks consist of the Ivittuut, Kvanefjord, Bjørnesund, Sermilik, Fiskefjord and Maniitsoq (Fig. 1). Each tectonic block is made of a southerly upper and a northerly lower zone (Windley & Garde, 2009). These blocks are composed predominantly of TTG orthogneisses containing numerous layers of anorthosite-bearing layered intrusions and amphibolite facies metavolcanic rocks.

2.2. Superior Province of Canada

The Archaean Superior Province of Canada consists of approximately east-west-striking TTG dominated-plutonic, greenstone-granitoid, high-grade TTG-gneissic and meta-sedimentary subprovinces (Fig. 2) (Card & Ciesielski, 1986; Stott, 1997; Percival et al., 2012). These subprovinces represent a tectonic collage of numerous fragments of continental blocks, oceanic island arcs, oceanic plateaus and orogenic flysch deposits. These lithotectonic terrains were assembled through subduction-driven, >1500 km long, accretionary and collisional processes, which took place diachronously from north to south between 2720 and 2680 Ma (Stott, 1997; Percival et al., 2012). Layered intrusions consisting mainly of gabbro, anorthosite and ultramafic rocks are exposed in many areas particularly in the northern Abitibi and the western Wabigoon greenstone-granitoid subprovinces and the North Caribou terrane (see Fig. 3 in Percival et al., 2012). Like those in the Archaean craton of southern West Greenland, the anorthosite-bearing layered intrusions in the Superior Province display well-preserved megacrystic textures (Ashwal, 1993) and are spatially and temporally associated with tholeiitic to calc-alkaline basalt-dominated volcanic rocks, and are intruded by syn- to post-tectonic TTGs (Davis, Sutcliffe, & Trowell, 1988; Bédard, Leclerc, Harris, & Goulet, 2009; Leclerc et al., 2011; Wu et al., 2016; Polat, Frei, Longstaffe, & Woods, 2017).

3. Summary of the geological and geochemical characteristics

3.1. West Greenland

An assemblage of leucogabbro and anorthosite is spatially and temporally associated with the ca. 3075 Ma Ivisaartoq greenstone belt and is intruded by ca. 2963 Ma old tonalites and granodiorites (Fig. 1) (Chadwick, 1985, 1990; Friend & Nutman, 2005; Polat et al., 2008). In addition, gabbros in the Ivisaartoq belt contain up to 15 cm long, deformed anorthositic inclusions (xenoliths), consisting primarily (>90%) of Ca-rich plagioclase and 5-10% amphibole (Fig. 5a, b; Polat et al., 2008). These xenoliths are interpreted to be anorthositic cumulates that were transported to the oceanic crust by upwelling gabbroic magmas. The xenoliths display Th- and LREE-enriched trace element patterns with large positive Eu but negative Nb and Ti anomalies (Fig. 6a), and have large positive initial ε_{Nd} (+4.8 to +6.0) values, consistent with a long-term depleted mantle source (Polat et al., 2008). Volcanic and intrusive rocks of the Ivisaartoq greenstone belt share the geochemical characteristics of Phanerozoic subduction zone magmas (Polat et al., 2008; Ordóñez-Calderón et al., 2009; Szilas et al., 2016).

The Mesoarchaean Naajat Kuuat Anorthosite Complex in southern West Greenland is composed of megacrystic anorthosite and leucogabbro, gabbro and ultramafic rocks, and is spatially associated with metavolcanic amphibolites (Fig. 1) (Hoffmann, Svahnberg, Piazolo, Scherstén, & Münker, 2012). The meter- to kilometer-long slices of the Naajat Kuuat Anorthosite Complex are interleaved with the intrusive TTGs. The anorthosites have arc-like trace element patterns, whereas the ultramafic rocks and metavolcanic amphibolites display MORB- to arc-like geochemical characteristics (Hoffmann, Svahnberg, Piazolo, Scherstén, & Münker, 2012). The anorthosites (εNd=+1.6 to +3.6; εHf=+2.5 to +5.8), ultramafic rocks (εNd=+0.4 to +2.0; εHf=+4.2 to +5.6) and amphibolites (εNd=+1.7 to +3.7; εHf=+1.6 to +5.3) have depleted mantle Nd and Hf isotopic compositions. On the basis of field observations and geochemical data, the Naajat Kuuat Anorthosite Complex and spatially associated amphibolites and TTG are interpreted to have formed in a suprasubduction zone setting (Hoffmann, Svahnberg, Piazolo, Scherstén, & Münker, 2012).

The ca. 2970 Fiskenæsset Anorthosite Complex, Western Greenland, is probably the largest and best-preserved Archaean anorthosite-bearing layered intrusion in the world, consisting of *ca.* 550 m-thick cumulate layers of anorthosite, leucogabbro, gabbro and hornblende-bearing ultramafic rocks (Figs. 3, 4) (Windley, Herd, & Bowden, 1973; Windley & Smith, 1974; Myers, 1985; Polat et al., 2009; Polat, Frei, Scherstén, & Appel, 2010, Polat et al., 2011; Polat et al., 2012; Rollinson, Reid, &

Windley, 2010; Huang, Polat, Fryer, Appel, & Windley, 2012; Huang, Fryer, Polat, & Pan, 2014). Field characteristics indicate that the Fiskenæsset Anorthosite Complex was emplaced into Mesoarchaean oceanic crust as multiple sills and dykes of magma and crystal mush, and is intruded by 2950-2750 Ma TTGs (Polat, Frei, Scherstén, & Appel, 2010; Polat et al., 2011; Polat et al., 2012; Huang, Polat, & Fryer, 2013). The Fiskenæsset anorthosites and leucogabbros display diverse REE patterns with variable La/Sm_{cn} and Gd/Yb_{cn} ratios, and have variably negative Nb and Ti but positive Eu anomalies (Polat et al., 2009; Polat et al., 2011; Huang, Polat, Fryer, Appel, & Windley, 2012). All rock types in the complex share the trace element characteristics of modern subduction zone igneous rocks, and have depleted mantle Nd (average initial $\varepsilon Nd=+3.3$), Pb and O primitive isotope ($\delta^{18}O=5.8\pm0.5‰$) compositions (Polat et al., 2009; Polat, Frei, Scherstén, & Appel, 2010; Polat et al., 2011; Huang, Polat, Fryer, Appel, & Windley, 2012; Polat et al., 2014; Polat & Longstaffe, 2014).

For this study, we analysed seven samples of megacrystic plagioclase from the leucogabbros of the Sinarssuk area (Fig. 1; Table 2). These plagioclase megacrysts have small variations in SiO_2 (46.7–48.2 wt.%), CaO (14.9–16.2 wt.%), and Al_2O_3 (31.9–3.5 wt.%) (Table 2). They have low MgO (0.18–0.33 wt.%), Fe_2O_3 (0.48–1.1 wt.%), TiO_2 (0.01-0.02 wt.%) and Na_2O (1.65-2.55 wt.%) contents. Mg-numbers span from 37 to 52 (Table 2). Anorthite (An%) contents vary from 78 to 86. Al_2O_3/TiO_2 (1440–4440) ratios are extremely super-chondritic.

The Sinarssuk megacrystic plagioclase samples are characterized by strongly fractionated REE patterns (La/Sm_{cn}=3.0–13.9; La/Yb_{cn}=6.2–83.7; Gd/Yb_{cn}=1.79–4.92), and positive Eu (Eu/Eu*=2.91–8.3) anomalies (Fig. 6b; Table 2). Cerium anomalies are minor to absent (Ce/Ce*=0.96–1.05). On the N-MORB-normalized diagram, they have large positive Pb (Pb/Pb*=186–3740), and negative Nb (Nb/Nb*=0.06–0.55) and Ti (Ti/Ti*=0.13-0.29) anomalies. Zirconium anomalies (Zr/Zr*=0.36-6.65) vary from negative to positive.

3.2. Superior Province

The Superior Province contains several well-preserved Neoarchaean anorthosite complexes including the Bad Vermilion Lake, Doré Lake, Shawmere, Pipestone, Pikwitonei and Bird River complexes (Ashwal, 1993; Peck, Messing, Halden, & Chandler, 1998; Gilbert, 2007; Yang, Gilbert, & Houlé, 2012). We have high-precision trace element data only for the Bad Vermilion Lake and Doré Lake complexes (Zhou et al., 2016; Polat, Frei, Longstaffe, & Woods, 2017). Accordingly, we focus on these two complexes.

The Bad Vermilion Lake Anorthosite Complex is located in the western Wabigoon subprovince of the western Superior Province (see Ashwal, Morrison, Phinney, & Wood, 1983; Percival et al., 2012; Zhou et al., 2016). It consists predominantly of anorthosite, leucogabbro and gabbro and intrudes the 2720 Ma tholeiitic to calc-alkaline volcanic rocks of the Bad Vermilion Lake greenstone belt (Davis, Sutcliffe, & Trowell, 1988; Blackburn, John, Ayer, & Davis, 1991; Zhou et al., 2016). The Bad Vermilion Anorthosite Complex is intruded by ca. 2716 Ma granitic rocks (Ashwal, Morrison, Phinney, & Wood, 1983; Zhou et al., 2016). The complex has depleted mantle-like Nd (εNd=ca. +2) and near-primitive O (δ^{18}O = +5.5 to +6.7 ‰) isotope signatures and subduction zone-like trace element patterns (Fig. 6c; Ashwal, Morrison, Phinney, & Wood, 1983; Zhou et al., 2016). The spatially associated mafic to felsic volcanic rocks with the complex also have subduction zone trace element characteristics (Wu et al., 2016).

The ca. 2728 Ma Doré Lake Complex is located in the northeastern segment of the Northern Volcanic Zone of the Abitibi subprovince and is composed predominantly of megacrystic anorthosite and leucogabbro, and gabbro (Daigneault, ST-Julien, & Allard, 1990; Bédard, Leclerc, Harris, & Goulet, 2009; Leclerc et al., 2011; Polat, Frei, Longstaffe, & Woods, 2017). The complex intrudes the basalt-dominated volcanic and sedimentary rocks of the Roy Group and is in turn intruded by the 2714 Ma tonalitic Chibougamau pluton (Ludden, Francis, & Allard, 1984; Daigneault, ST-Julien, & Allard, 1990; Mortensen, 1993; Bédard, Leclerc, Harris, & Goulet, 2009; Leclerc et al., 2011). The Nd (εNd=+ 2.6 to +5.0) and O (δ^{18}O=+6.05 to +7.85‰) isotope systematics are consistent with a depleted mantle source (Polat, Frei, Longstaffe, & Woods, 2017). Like the Bad Vermilion Lake anorthosites and spatially associated volcanic rocks, the Doré Lake anorthosites and spatially associated volcanic rocks (see Figs 8-10 in Leclerc et al., 2011; Polat, Frei, Longstaffe, & Woods, 2017) also have subduction zone trace element signatures (Fig. 6d), although Leclerc et al. (2011) do not attribute the origin of Th- and LREE-enriched patterns with negative Nb, Ta and Ti anomalies in the tholeiitic to calc-alkaline volcanic rocks to Archaean subduction zone processes.

4. Geodynamic origin of Archaean anorthosites

Numerous studies on the thermal history of the Earth suggest that the ambient temperature of the Archaean mantle (1500–1600°C) was 200-300 °C higher than today's mantle (1300–1400 °C) (e.g., Nisbet, Cheadle, Arndt, & Bickle, 1993; Korenaga, 2008; Davies, Sutcliffe, & Trowell, 2009; Lee, Luffi, Plank, Dalton, & Leeman, 2009; Herzberg, Condie, & Korenaga, 2010). The higher mantle temperatures beneath the Archaean oceanic spreading centres would have produced 25-35% partial melting, resulting in three to four times more voluminous basaltic magma than the 7-10% partial melting beneath present-day spreading centres (see McKenzie & Bickle, 1988; Herzberg, 2004; Herzberg, Condie, & Korenaga, 2010). Such high degrees of partial melting would have generated 25-35 km thick oceanic crust, in contrast to the 7-10 km thick crust produced at modern ocean ridges (Sleep & Windley, 1982; Bickle, 1986; Herzberg, Condie, & Korenaga, 2010). Although petrological models predicting higher mantle temperatures for the Archaean are based on the composition of non-arc basalts (e.g., Lee, Luffi, Plank, Dalton, & Leeman, 2009; Herzberg, Condie, & Korenaga, 2010), the presence of arc picrites, boninites and high-Mg andesites in Archaean greenstone belts might also imply higher ambient mantle temperatures beneath Archaean arcs and backarcs (Polat & Kerrich, 2006). We propose that 25-35% degrees of partial melting in the Archaean upper mantle would have resulted in a large volume of basaltic magmas underplating rifting arcs and/or backarc basins, generating large, shallow magma chambers (Fig. 7). Higher geothermal gradients in the Archaean oceanic crust would have allowed these shallow magma chambers to cool slowly, providing optimal conditions for differentiation and stratification to produce cumulates of dunite, peridotite, chromitite, pyroxenite, (±hornblendite), gabbro, leucogabbro and anorthosite (Fig. 7) (Polat et al., 2009; Namur et al., 2015). The Fiskenæsset Complex contains numerous small-scale (50 centimetres to 5 meters thick) examples of differentiated sills representing smaller versions of magma chambers that solidified to form such cumulate layers, including hornblendite, in the oceanic crust (Fig. 4a, b; see Myers, 1985; Polat et al., 2011).

Archaean plagioclase megacrysts, including those in the Fiskenæsset Complex, are typically characterized by high-Ca content ($An_{70\text{-}93}$) (see Ashwal, 2010; Ashwal & Bybee, 2017). Previous studies have shown that plagioclase grains in the anorthosites and leucogabbros of the Fiskenæsset Complex typically have high anorthite (An) contents, ranging between 75 and 98% (Windley & Smith, 1974; Myers & Platt 1977; Rollinson, Reid, & Windley, 2010; Huang, Fryer, Polat, & Pan, 2014). The plagioclase megacrysts from the Sinarssuk area of the Fiskenæsset region (Figs. 1, 3) also have high-Ca contents (An_{78-86}). Additional analyses of plagioclase in leucogabbros and hornblendites on the island of Qeqertarssuatsiaq also indicate high An contents (An_{66-91}) (see Data Repository Table 1). These high An contents are attributed to hydrous parental melts in a subduction zone environment (see Müntener, Kelemen, Grove, 2001; Tagaki, Sato, & Nakagawa, 2005; Ashwal, 2010).

Virtually all rock types and structures that are associated with Archaean anorthosite-bearing layered intrusions (Myers, 1976; Myers, 1985; Daigneault, ST-Julien, & Allard, 1990; Davis, Sutcliffe, & Trowell, 1988; Polat, Wang, & Appel, 2015; Wu et al., 2016) have analogues in Phanerozoic convergent plate margins and orogenic belts. Although the details of tectonic processes that produced Archaean anorthosite-bearing layered intrusions and spatially associated volcanic rocks and TTG intrusions remain to be determined, trace element data and field observations indicate that their origin can be explained best by subduction zone tectonic processes (Chown, Daigneault, Mueller, & Mortensen, 1992; Mueller, Daigneault, Mortensen, & Chown, 1996; Daigneault, Mueller, Chown, 2002; Windley & Garde, 2009; Percival et al., 2012; Polat et al., 2009; Polat et al., 2011; Polat, Frei, Longstaffe, & Woods, 2017). Available Nd and O isotope data for Archaean anorthosite complexes suggest that they originated from long-term depleted mantle sources that were overprinted by subduction-derived melts and/or fluids (Polat et al., 2008; Polat, Frei, Scherstén, & Appel, 2010; Polat, Frei, Longstaffe, & Woods, 2017; Polat & Longstaffe, 2014; Zhou et al. 2016). None of the Archaean anorthosite-bearing layered intrusions discussed in this contribution displays evidence for extensive crustal contamination. Hence, the Th- and LREE-enriched and Nb- and Ti-depleted trace element patterns in these rocks (Fig. 6) reflect subduction zone geodynamic processes rather than emplacement into older continental crust. Collectively, we interpret the anorthosite-bearing layered intrusions in the Archaean craton of western Greenland and the Superior Province as remnants of rifted oceanic arcs or backarc basins (Fig. 7).

5. Anorthosite-bearing layered intrusions and the nature Archaean oceanic crust

Given their absence in the Phanerozoic rock record, Archaean anorthosite-bearing layered intrusions and associated greenstone belts are not generally considered part of oceanic crust because they do not have a Penrose-type ophiolite lithological association. Thus, these rock associations are not interpreted to be ophiolites (Hamilton, 1998; Stern, 2005; Kamber, 2015). Recent studies on Phanerozoic ophiolites and Archaean greenstone belts have shown that the original Penrose ophiolite definition (Anonymous, 1972) is too simplistic and has major limitations for understanding the evolution of the oceanic crust and its diversity in the rock record (Kusky, 2004; Şengör & Natal'in, 2004; Dilek & Furnes, 2011; Kusky et al., 2013; Furnes, Dilek, & de Wit, 2015). Therefore, this definition is not recommended to be used as a guide to define ophiolites in Archaean terrains that are typically characterized by polyphase deformation, and multiple generations of metamorphism and granitoid intrusion. Given that the Penrose ophiolite definition cannot be readily applied to the Precambrian rock record, Dilek & Furnes (2011) proposed a broad definition ophiolite as "suites of temporally and spatial associated ultramafic to felsic rocks related to separate melting episodes and processes of magmatic differentiation in particular tectonic environments". On the basis of new definition, ophiolites are divided into two major types: (1) subduction-related ophiolites that form in backarc, forearc and arc tectonic settings; and (2) subduction-unrelated ophiolites that originate in rifted continental margins, mid-ocean ridges and plume-derived oceanic plateaus. The subduction-related ophiolites constitute about 85% of the ophiolites in the rock record (Furnes et al., 2015), reflecting mainly their biased preservation. Because of its buoyancy, suprasubduction crust is less prone to the subduction and recycling than “normal” oceanic crust produced along mid-ocean ridges. Most Archaean greenstone belts have Phanerozoic subduction zone-like lithological and geochemical characteristics, representing dismembered fragments of oceanic island arcs and backarcs (Furnes, Dilek, & de Wit, 2015).

On the basis of their lithological and geochemical characteristics, we interpret Archaean anorthosite-bearing layered intrusions and spatially associated greenstone belts to be subduction-related Archaean ophiolites using the new ophiolite concept developed by Dilek and Furnes (2011) and Furnes, Dilek, & de Wit (2015). These rock associations represent relict fragments of Archaean suprasubduction zone (arc-backarc-forearc) crust, marking the closure of ocean basins and formation of suture zones in Archaean orogenic belts (Polat, Frei, Longstaffe, & Woods, 2017).

Modern oceanic lithosphere forming at spreading centres consists generally of a mantle section (dunite, lherzolite, harzburgite) at the bottom, mafic to ultramafic cumulates (gabbros, pyroxenites) in the middle, and a mafic crustal section (isotropic gabbros, sheeted dykes and basalts) at the top. The thickness of the mafic rocks in modern oceanic crust and Phanerozoic ophiolites varies between 5 and 10 km, which is much smaller than the predicted 25-35 km thickness of Archaean oceanic crust (Sleep & Windley, 1982; Herzberg, Condie, & Korenaga, 2010). In contrast to Phanerozoic oceanic crust, Archaean oceanic crust was likely composed of an association of 25-35 km thick basaltic flows and sills of gabbros, anorthosites, leucogabbros and differentiated ultramafic rocks (Fig. 7b) (Dilek & Polat, 2008).

6. Magma chamber dynamics and the origin of megacrystic plagioclase

Textural analyses of layered intrusions and theoretical studies of magma chamber dynamics suggest that if a magmatic system with a single mineral, like plagioclase growing in a liquid at the top of a magma chamber, remains at high temperatures close to the liquidus of that mineral, large crystals will develop at the expense of small ones (Ostwald ripening), resulting in a megacrystic grain size (Higgins, 2005, 2011). Field observations of the Fiskenæsset Complex indicate that plagioclase crystals separated from the residual liquid and floated to the top of the magma chamber, forming a crystal mush of leucogabbro and anorthosite (Fig. 4a, b, c; see Scoates, 2002; Higgins, 2005; Namur et al., 2011). Floatation of plagioclase was likely facilitated by the presence of denser residual liquid, which mostly crystallized to hornblende (Figs. 3, 4). The presence of plagioclase laminations, erosional surfaces, slump structures and trough layers (Myers, 1985), and the injection of plagioclase crystal mush into a gabbroic magma (Fig. 4d-f) are consistent with a dynamic, vigorously convecting magma chamber (see Higgins, 2005; Namur et al., 2015). The presence of amphibole inclusions in chromite grains in the Fiskenæsset Complex is attributed to a hydrous magma composition (Rollinson, Reid, & Windley, 2010; Polat, 2012). The Fiskenæsset Complex provides field evidence for most stages of crystallization of plagioclase in hydrous melts to form megacrystic anorthosites and leucogabbros (Fig. 3). This hydrous magmatic system likely remained at high temperatures (1000-1200 °C) for a long period of time, resulting in the formation of megacrystic (2-15 cm in diameter) plagioclase grains. Plagioclase grain size varies from 2 mm to 30 cm and some megacrysts appear to have formed by coalescence of smaller megacrysts (Figs. 3 and 8). Most plagioclase grains display field and petrographic evidence for metamorphic recrystallization (Figs. 8). The continuity of albite twinning for 6-8 cm in the least deformed and recrystallized megacrysts in samples 508144 and 508146 collected from the least-deformed outcrops in the Sinarssuk area (Figs. 1, 9; Table 2), however, clearly demonstrates their formation as single crystals, rather than coalesced, in the magma chamber. The megacrystic magma either solidified in place or was transported as crystal mush into the overlying oceanic crust to form sills, dykes or pods of anorthosites and leucogabbros (Fig. 7). These plagioclase megacrysts grew further by interaction with either new melts and/or melts expelled from the lower parts of the magma chamber, producing grains up to 30 cm in length (Fig. 3). Collectively, large grain sizes in Archaean megacrystic anorthosites and leucogabbros can be interpreted as the product of slow cooling conditions close to the plagioclase liquidus temperatures that stemmed from the higher geothermal gradients in the Archaean oceanic crust.

7. Conclusions

Anorthosite-bearing layered intrusions in the Archaean craton of southern West Greenland and the Superior Province of Canada were emplaced into basalt-dominated greenstone belts, and were intruded by syn- to post-tectonic granitoids. All these three rock associations share the trace element signatures of modern subduction-related magmas, suggesting that they originated in a suprasubduction zone setting, representing Archaean subduction-related ophiolites. Anorthosite-bearing layered intrusions and spatially associated greenstone belts are interpreted as fragments of suture zones, marking the closure of Archaean ocean basins. These intrusions in Greenland and Canada are mostly located close to the major tectonic boundaries separating different tectonic blocks/terranes (Figs. 1, 2), suggesting a close relationship between the formation of anorthosite-bearing layered intrusions and major tectonic processes that led the amalgamation of different blocks/terranes.

Ashwal (2010) and Ashwal & Bybee (2017) addressed the temporality of anorthosites, showing that high-Ca (An=61–94%, average An=80%) megacrystic Archaean and massif-type Proterozoic anorthosites (An=30–70%, average An=53%) are restricted in space and time, whereas continental layered mafic intrusions and ophiolites do not show clear time-restriction. Field studies indicate that Archaean anorthosites originated mostly in oceanic settings and are spatially and temporally associated with basalt-dominated greenstone belts, whereas Proterozoic counterparts are spatially associated with granitoid rocks and thought to have formed in continental arcs. Anorthosites in Phanerozoic ophiolites (Table 1) originated mainly in suprasubduction zone settings (e.g., oceanic arcs, backarc basins, and forearcs) and are characterized by millimetre grain size and centimetre to decimetre thick layers, in contrast to hundreds of meters to several kilometres thick Archaean megacrystic anorthosites.

We suggest that changes in the nature of anorthosites occurring in oceanic settings in Archaean and post-Archaean times reflect the thermal evolution of the Earth. Irreversible heat loss of the Earth led to upper mantle cooling by the end of the Archaean to a level at which it could no longer produce 25-35% partial melting, except within mantle plumes, beneath oceanic arcs and spreading centres. Large degrees of partial melting in the Archaean mantle led to the formation of mineralogically-stratified, km-scale magma chambers beneath spreading centres and magmatic arcs. These magma chambers consisted mainly of olivine-, pyroxene-, hornblende-, and plagioclase-rich crystal mushes (Fig. 7), and cooled slowly in response to higher geothermal gradients in the oceanic crust and magmatic arcs, providing optimum petrological conditions for the formation of megacrystic plagioclase in anorthosites and leucogabbros (Fig. 7). In addition to higher mantle temperatures, the presence of water in Archaean suprasubduction zone magmas might have played an important role in the formation of plagioclase megacrysts by enhancing the magma cooling time and element diffusion rates. Because of declining ambient mantle temperatures and geothermal gradients in the oceanic crust, the generation of large, mineralogically stratified magma chambers decreased and eventually ceased by the end of the Archaean Eon, leading to the termination of the formation of high-Ca megacrystic anorthosites in post-Archaean oceanic environments.

Acknowledgments

Tim Kusky, Claude Herzberg and Michael Higgins are acknowledged for their insightful, helpful and constructive comments on the previous version of the paper. This research is supported by NSERC grants to A. Polat and F.J. Longstaffe.

References

Anonymous (1972). Penrose field conference on Ophiolites. *Geotimes, 17,* 24–25.

Arvin, M., Babaei, A., Ghadami, G., Dargahi, S., & Ardekani, A. S. (2005). The origin of the Kahnuj ophiolitic complex, SE of Iran; constraints from whole rock and mineral chemistry of the Bande-Zeyarat gabbroic complex. *Ofioliti, 30,* 1–14.

Ashwal, L.D. (1993). Anorthosites: Berlin, Germany, Minerals and Rocks Series 21, Springer-Verlag, p. 422.

Ashwal, L. D. (2010). The temporality of anorthosites. *The Canadian Mineralogist,* 48, 711–728.

Ashwal, L. D., & Bybee, G. M. (2017). Crustal evolution and the temporality of anorthosites. *Earth-Science Reviews, 173,* 307–330.

Ashwal, L. D., Morrison, D. A., Phinney, W. C., & Wood, J. (1983). Origin of Archean anorthosites: evidence from the Bad Vermilion Lake Anorthosite Complex, Ontario. *Contributions to Mineralogy and Petrology, 82,* 259–273.

Austrheim, H., & Prestvik, T. (2008). Rodingitization and hydration of the oceanic lithosphere as developed in the Leka Ophiolite, north-central Norway. *Lithos, 104,* 177–198.

Bédard, J. H., Leclerc, F., Harris, L. B., & Goulet, N. (2009). Intra-sill magmatic evolution in the Cumming Complex, Abitibi greenstone belt: Tholeiitic to calc-alkaline magmatism recorded in an Archean subvolcanic conduit system. *Lithos, 111,* 47–71.

Bickle, M. J. (1986). Implications of melting for stabilization of the lithosphere and heat loss in the Archean. *Earth and Planetary Science Letters, 80,* 314–324.

Blackburn, C. E., John, G. W., Ayer, J., & Davis, D. W. (1991). Wabigoon Subprovince. In P. C. Thurston, H. R. Williams, R. H. Sutcliffe, & G. M. Stott (Eds.), *Geology of Ontario* (Special Vol. 4, Part 1, pp. 303–381), Sudbury: Ontario Geological Survey.

Borodina, E. V., Egorova, V. V., & Izokh, A. E. (2004). Petrology of Ordovician collision-related layered peridotite-gabbro intrusions (exemplified by the Mazhalyk Intrusion, southeastern Tuva). *Russian Geology and Geophysics,* 45, 1025–1042.

Boudier, F., & Nicolas, A. (2011a). Axial melt lenses at oceanic ridges; a case study in the Oman Ophiolite. *Earth and Planetary Science Letters, 304,* 313–325.

Boudier, F. I., & Nicolas, A. J. (2011b). Anorthosites in Oman Ophiolite crust, a clue to crust origin at a fast spreading ridge. American Geophysical Union Fall Meeting, San Francisco, Abstract V21B–2494.

Card, K. D., & Ciesielski, A. (1986). Subdivisions of the Superior Province of the Canadian Shield. *Geoscience Canada, 13,* 5–13.

Chadwick, B. (1985). Contrasting styles of tectonism and magmatism in the late Archean crustal evolution of the northeastern part of the Ivisaartoq region, inner Godthåbsfjord, southern West Greenland. *Precambrian Research, 27,* 215-238.

Chadwick, B., (1990). The stratigraphy of a sheet of supracrustal rocks within high-grade orthogneisses and its bearing on late Archean structure in southern West Greenland. *Journal of Geological Society London, 147,* 639-652.

Chown, E. H,, Daigneault R., Mueller, W., & Mortensen, J. K. (1992). Tectonic evolution of the Northern Volcanic Zone, Abitibi Belt, Quebec. *Canadian Journal of Earth Sciences, 29,* 2211–2225.

Daigneault, R., Mueller, W. U., Chown, E. H. (2002). Oblique Archean subduction: accretion and exhumation of an oceanic arc during dextral transpression, Southern Volcanic Zone, Abitibi Subprovince Canada. *Precambrian Research, 115,* 261–290.

Daigneault, R., ST-Julien, P., & Allard, G.O. (1990) Tectonic evolution of the northeast portion of the Abitibi greenstone belt, Chibougamau area, Quebec. Canadian Journal of Earth Sciences, 27, 1714–1736.

Davis, D. W., Sutcliffe, R. H., & Trowell, N. F. (1988). Geochronological constraints on the tectonic evolution of a late Archean greenstone belt, Wabigoon subprovince, northwest Ontario. *Precambrian Research, 39,* 171–191.

Davies, G. F. (2009). Effect of plate bending on the Urey ratio and the thermal evolution of the mantle. *Earth and Planetary Science Letters, 287,* 513–518.

Dilek, Y., & Furnes, H. (2011). Ophiolite genesis and global tectonics: geochemical and tectonic fingerprinting of ancient oceanic lithosphere. *Geological Society of America Bulletin, 123,* 387–411.

Dilek, Y., & Polat, A. (2008). Suprasubduction zone ophiolites and Archean tectonics. *Geology, 36,* 431-432.

Dymek, R. F., & Owens, B. R. (2001). Chemical assembly of Archean anorthosites from amphibolite- and granulite-facies terranes, SW Greenland. *Contributions to Mineral and Petrology, 141,* 513-528.

Dziggel, A., Diener, J.F.A., Kolb, J., & Kokfelt, T.F., 2014. Metamorphic record of accretionary processes during the Neoarchean: The Nuuk region, Southern West Greenland. *Precambrian Research, 242,* 22–38.

Eyuboglu, Y., Dilek, Y., Bozkurt, E., Bektas, O., & Rojay, B. (2010). Structure and geochemistry of an Alaskan-type ultramafic-mafic complex in the eastern Pontides, NE Turkey. *Gondwana Research, 18,* 230–252.

Friend, C. R. L., & Nutman, A. P. (2005). New pieces to the Archean jigsaw puzzle in the Nuuk region, southern West Greenland: steps in transforming a simple insight into a complex regional tectonothermal model. *Journal of the Geological Society, London, 162,* 147–162.

Fazlnia, A., & Alizade, A. (2013). Petrology and geochemistry of the Mamakan gabbroic intrusions, Urumieh (Urmia), Iran; magmatic development of an intro-oceanic arc. *Periodico di Mineralogia, 82,* 263–290.

Furnes, H., Dilek, Y., & de Wit, M. (2015). Precambrian greenstone sequences represent different ophiolite types. *Gondwana Research, 27,* 649–685.

Garde, A. A. (2007). A Mid-Archean island arc complex in the eastern Akia terrane, Godthåbsfjord, southern West Greenland. *Journal of the Geological Society, London, 164,* 565–579.

Gilbert, H. P. (2007). Stratigraphic investigations in the Bird River greenstone belt, Manitoba (part of NTS 52L5, 6); In Report of Activities 2007. Manitoba Science, Technology, Energy and Mines, Winnipeg, Manitoba Geological Survey, p. 129–143.

Hamilton, W. B., (1998). Archean magmatism and deformation were not products of plate tectonics. *Precambrian Research, 91,* 143–179.

Hawkins, J. W. (2007). Geology of western Pacific ophiolites and suprasubduction zone systems; insight to origin of cordilleran terranes. Geological Society of America, Cordilleran Section, 103rd Annual meeting, Colorado, Geological Society of America Annual Meeting, Abstract 39-80.

Henares, S., Gonzalez-Jimenez, J. M., Gervilla, F., Proenza, J. A., Rodriguez, A. C., & Gonzalez-Ponton, R.B. (2010). The chromitites of the Camaguey ophiolite complex, Cuba; an example of Al-rich Chromitites. *Boletin de la Sociedad Geologica Mexicana, 62,* 173-185.

Herzberg, C. (2004). Geodynamic information in peridotite petrology. *Journal of Petrology, 45,* 2507–2530.

Herzberg, C., Condie, K., & Korenaga, J. (2010). Thermal history of the Earth and its petrological expression. *Earth and Planetary Science Letters, 292,* 79–88.

Higgins, M. D. (2005). A new model for the structure of the Sept Iles intrusive suite, Canada. *Lithos, 83,* 199–213.

Higgins, M. D. (2011). Textural coarsening in igneous rocks. *International Geology Review, 53,* 354-376.

Hoffmann, J. E., Svahnberg, H., Piazolo, S., Scherstén, A., & Münker, C. (2012). The geodynamic evolution of Mesoarchean anorthosite complexes inferred from the Naajat Kuuat Complex, southern West Greenland. *Precambrian Research, 196–197,* 149–170.

Huang, H., Fryer, B. J., Polat, A., & Pan, Y. (2014). Amphibole, plagioclase and clinopyroxene geochemistry of the Archean Fiskenæsset Complex at Majorqap qâva, southwestern Greenland: Implications for Archean petrogenetic and geodynamic processes. *Precambrian Research, 247,* 64–91.

Huang, H., Polat, A., Fryer, B. J., Appel, P. W. U., & Windley, B. F. (2012). Geochemistry of the Mesoarchean Fiskenæsset Complex at Majorqap qâva, SW Greenland: Evidence for two different magma compositions. *Chemical Geology, 314-317,* 66–82.

Huang, H., Polat, A., & Fryer, B. J. (2013). Origin of the Archean tonalite–trondhjemite–granodiorite (TTG) suites and granites in the Fiskenæsset region, southern West Greenland: implication for the continental growth. *Gondwana Research, 23,* 452–470.

Jian, P., Liu, D., Kroener, A., Windley, B. F., & Shi, Y. (2010). Evolution of a Permian intraoceanic arc-trench system in the Solonker suture zone, Central Asian orogenic belt, China and Mongolia. *Lithos, 118,* 169–190.

Jian, P., Liu, D., Zhang, Q., Zhang, F., & Yurup, S. (2003). SHRIMP dating of ophiolite and leucocratic rocks within ophiolite. *Earth Science Frontiers, 4,* 439–456.

Jian, P, Wang, X., He, L., & Wang, C. (1999). U-Pb zircon dating of anorthosite and plagiogranite from the Jinshajiang ophiolite belt, China. *Acta Petrologica Sinica, 15,* 590–593.

Kamber, B. S. (2015). The evolving nature of terrestrial crust from the Hadean, through the Archaean, into the Proterozoic. *Precambrian Research, 258,* 48–82.

Kadarusman, A., Miyashita, S., Maruyama, S., Parkinson, C., & Ishikawa, A. (2004). Petrology, geochemistry and paleogeographic reconstruction of the East Sulawesi Ophiolite, Indonesia. *Tectonophysics, 392,* 55–83.

Khan, M. A., Jan, M. Q., Windley, B. F., Tarney, J., & Thirlwall, M. F. (1989). The Chilas mafic-ultramafic igneous complex; the root of the Kohistan island arc in the Himalaya of northern Pakistan. In L.M. Jr. Lawrence, & R. J. Lillie (Eds.), *Tectonics of the western Himalayas* (Vol. 232, pp. 75-94), Colorado, Geological Society of America, Special Paper.

Kisters, A.F.M., van Hinsberg, V.J., & Szilas, K., 2012. Geology of an Archaean accretionary complex — the structural record of burial and return flow in the Tartoq Group of South West Greenland. *Precambrian Research, 220–221,* 107–122.

Kite, L.C., & Stoddard, E. F. (1984). The Halifax County Complex; oceanic lithosphere in the eastern North Carolina Piedmont. *Geological Society of America Bulletin, 95,* 422–432.

Komor, S.C., & Elthon, D. (1990). Formation of anorthosite-gabbro rhythmic phase layering; an example at North Arm Mountain, Bay of Islands Ophiolite. *Journal of Petrology, 31,* 1–50.

Korenaga, J. (2008). Urey ratio and the structure and evolution of Earth's mantle. *Reviews of Geophysics, 46,* RG2007.

Kusky, T. M. (2004). Epilogue: What if anything have we learned about Precambrian ophiolites and early Earth processes? In T. M. Kusky (Ed.), *Precambrian Ophiolites and Related Rocks*, *Developments in Precambrian Geology,* (Vol. 13, pp. 727–637), Amsterdam, Elsevier.

Kusky, T. M., Windley, B. F., Safonova, I., Wakita, K., Wakabayashi, J., Polat, A., & Santosh, M. (2013). Recognition of plate stratigraphy in accretionary orogens through Earth history: A record of 3.8 billion years of sea floor spreading, subduction, and accretion. *Gondwana Research, 24,* 501–547.

Leake, R. C., & Styles, M. T. (1984). Borehole sections through the Traboe hornblende schists, a cumulate complex overlying the Lizard peridotite. *Journal of the Geological Society, London, 141,* 41–52.

Leclerc, F., Bédard, J. H, Harris, L. B., McNicoll, V. J., Goulet, N., Roy, P., & Houle, P. (2011). Tholeiitic to calc-alkaline cyclic volcanism in the Roy Group, Chibougamau area, Abitibi Greenstone Belt — revised stratigraphy and implications for VHMS exploration. *Canadian Journal of Earth Sciences, 48,* 661–694.

Lee, C.-T. A., Luffi, P., Plank, T., Dalton, H. A., & Leeman, W. P. (2009). Constraints on the depths and temperatures of basaltic magma generation on Earth and other terrestrial planets using new thermobarometers for mafic magmas. *Earth Planetary Science Letters, 279,* 20–33.

Ludden J. N., Francis, D., & Allard, G. (1984). The geochemistry and evolution of the volcanic rocks of the Chibougamau region of the Abitibi metavolcanic belt. In J. Guha, E.H. Chown (Eds.), *Chibougamau—Stratigraphy and Mineralization* (Special Vol. 34, pp. 20–34), Canadian Institute of Mining and Metallurgy, Quebec City.

McKenzie, D., & Bickle, M. J. (1988). The volume and composition of melt generated by extension of the lithosphere. *Journal of Petrology, 29,* 625–679.

Mitsis, I., & Economou-Eliopoulos, M. (2001). Occurrence of apatite associated with magnetite in an ophiolite complex (Othrys), Greece. *American Mineralogist, 86,* 1143-1150.

Mortensen, J. K. (1993). U–Pb geochronology of the eastern Abitibi subprovince. Part 1: Chibougamau–Matagami–Joutel region. *Canadian Journal of Earth Sciences, 30,* 11–28.

Mueller, W., Daigneault, R., Mortensen, J., & Chown, E.H. (1996). Archean terrane docking: upper crust collision tectonics, Abitibi Greenstone Belt, Quebec, Canada. *Tectonophysics, 265,* 127–150.

Müntener, O., Kelemen, P. B., Grove, T. L. (2001). The role of H_2O during crystallization of primitive arc magmas under uppermost mantle conditions and genesis of igneous pyroxenites: an experimental study. *Contributions to Mineralogy and Petrology, 141,* 643–658.

Myers, J. S. (1976). Granitoid sheets, thrusting, and Archean crustal thickening in West Greenland. *Geology, 4,* 265-268.

Myers, J. S. (1985). Stratigraphy and structure of the Fiskenæsset Complex, southern West Greenland. Grønlands Geologiske Undersøgelse Bulletin 150, p. 72, Copenhagen.

Myers, J. S. (2001). Protoliths of the 3.7-3.8 Ga Isua greenstone belt, West Greenland. *Precambrian Research, 105,* 129–141.

Myers, J. S., & Platt, R. G. (1977). Mineral chemistry of layered Archaean anorthosite at Majorqap qava, near Fiskenæsset, southwest Greenland. *Lithos, 10,* 59-72.

Namur, O., Charlier, B., Pirard, C., Hermann, J., Liégeois, J.- P., & Vander Auwera, J. (2011). Anorthosite formation by plagioclase flotation in ferrobasalt and implications for the lunar crust. *Geochimica et Cosmochimica Acta, 75,* 4998-5018.

Namur, O., Abily, B., Bourdreau, A. F., Blandchette, F., Bush, J. W. M., Ceuleneer, G., Charlier, B., Donaldson, C. M., Duchesne, J.- C., Higgins, M. D., Morata, D., Nielsen, T. F. D., O'Driscoll, B., Pang, K. N., Peacock, T., Spandler, C. J., Toramaru, A., & Veksler, I.V. (2015). Igneous layering in magma chambers. In C. Bernard, O. Namur, R. Latypov, & T. Christian (Eds.), *Layered Intrusions*, New York, pp.75–152, Springer.

Newman, S., Stolper, E., & Stern, R. (2000) H_2O and CO_2 in magmas from the Mariana arc and back arc systems. Geochemistry, Geophysics, Geosystems – G3. 1999GC000027.

Nisbet, E. G., Cheadle, M. J., Arndt, N. T., & Bickle, M. J. (1993). Constraining the potential temperature of the Archaean mantle: a review of the evidence from komatiites. *Lithos, 30,* 291–307.

Nutman, A. P., Friend, C. R. L., & Bennett, V. C. (2002). Evidence for 3650-3600 Ma assembly of the northern end of the Itsaq Gneiss Complex, Greenland: Implication for early Archean tectonics. *Tectonics* 10.1029/2000TC001203.

Ordóñez-Calderón, J. C., Polat, A., Fryer, B., Appel, P. W. U., van Gool, J. A. M., Dilek, Y., & Gagnon, J. E. (2009). Geochemistry and geodynamic origin of Mesoarchean oceanic crust in the Ujarassuit and Ivisaartoq greenstone belts, SW Greenland. *Lithos, 113,* 133–157.

Owens, B. E. & Dymek, R. F. (1997). Comparative petrology of Archean anorthosites in amphibolite and granulite facies terranes, SW Greenland. *Contributions to Mineralogy Petrology, 128,* 371-384.

Parkinson, C. (1998). Emplacement of the East Sulawesi Ophiolite: evidence from subophiolite metamorphic rocks. *Journal of Asian Earth Sciences, 16,* 13–28.

Peck, D. C., Messing, C., Halden, N. M., & Chandler, C. (1998). New insights into the petrogenesis of the Pipestone Lake anorthosite complex and its Ti-V-Fe oxide deposits (parts of NTS 63I/5 and I/12). In Manitoba Energy and Mines, Geological Services, Winnipeg, Report of Activities, 1998, p. 127–134.

Percival, J. A., Skulski, T., Sanborn-Barrie, M., Stott, G. M., Leclair, A. D., Corkery, M. T., & Boily, M. (2012). Geology and tectonic evolution of the Superior Province, Canada. In J. A. Percival, F. A. Cook, & R. M. Clowes (Eds.), *Tectonic Styles in Canada*, (Vol. 49, pp. 321–378), Geological Association of Canada, Ottawa, The Lithoprobe Perspective, Special Paper.

Peterson, V., Ryan, J., Becker, A., Cochrane, D., & Collins, J. (2009). Petrogenesis and structure of the Buck Creek mafic-ultramafic suite, Southern Appalachians; constraints on ophiolite evolution and emplacement in collisional orogens. *Geological Society of America Bulletin, 121,* 615–629.

Phinney, W. C., Donald A. M., & David E. M. (1988). Anorthosites and related megacrystic units in the evolution of Archean crust. *Journal of Petrology, 29,* 1283–1323.

Polat, A. (2012) Growth of Archean continental crust in oceanic island arcs: Geology, v. 40, p. 383–384.

Polat, A., Frei, R., Appel, P. W. U., Dilek, Y., Fryer, B., Ordóñez-Calderón, J. C., & Yang, Z., (2008). The origin and compositions of Mesoarchean oceanic crust: Evidence from the 3075 Ma Ivisaartoq greenstone belt, SW Greenland. *Lithos, 100,* 293-321.

Polat, A., Appel, P. W. U., Fryer, B., Windley, B., Frei, R., Samson, I. M., & Huang, H. (2009). Trace element systematics of the Neoarchean Fiskenæsset anorthosite complex and associated meta-volcanic rocks, SW Greenland: Evidence for a magmatic arc origin. *Precambrian Research, 175,* 87-115.

Polat, A., Fryer, B. J., Appel, P. W. U., Kalvig, P., Kerrich, R., Dilek, Y., & Yang, Z. (2011). Geochemistry of anorthositic differentiated sills in the Archean (~ 2970Ma) Fiskenæsset Complex, SW Greenland: Implications for parental magma compositions, geodynamic setting, and secular heat flow in arcs. *Lithos, 123,* 50–72.

Polat, A., Fryer, B., Samson, I.M., Weisener, C., Appel, P. W. U., Frei, R., & Windley, B. F. (2012). Geochemistry of ultramafic rocks and hornblendite veins in the Fiskenæsset layered anorthosite complex, SW Greenland: Evidence for hydrous upper mantle in the Archean. *Precambrian Research, 214-215*, 124–153.

Polat, A., Frei, R., Longstaffe, F.J., & Woods, R. (2017). Petrogenetic and geodynamic origin of the Neoarchean Doré Lake Complex, Abitibi subprovince, Superior Province, Canada. *International Journal of Earth Sciences*. DOI: 10.1007/s00531-017-1498-1.

Polat, A., Frei, R., Scherstén, A., & Appel, P. W. U. (2010). New age (ca. 2970Ma), mantle source composition and geodynamic constraints on the Archean Fiskenæsset anorthosite complex, SW Greenland. *Chemical Geology, 277,* 1-20.

Polat, A., & Kerrich, R. (2006). Geochemical fingerprints of Archean hot subduction volcanic rocks: evidence for accretion and crustal recycling in a mobile tectonic regime. In K. Benn, J. C. Mareschal, & K.C. Condie (Eds.), *Archean Geodynamics and Environments* (Vol. 164, pp. 189-213), Washington: American Geophysical Union Geophysical Monograph Series.

Polat, A., & Longstaffe, F. J. (2014). A juvenile oceanic island arc origin for the Archean (ca. 2.97 Ga) Fiskenæsset Anorthosite Complex, southwestern Greenland: Evidence from oxygen isotopes. *Earth and Planetary Science Letters, 396,* 252-266.

Polat, A., Wang, L., & Appel, P. W. U. (2015). A review of structural patterns and melting processes in the Archean craton of West Greenland: Evidence for crustal growth at convergent plate margins as opposed to non-uniformitarian models. *Tectonophysics, 662,* 67–94.

Price, M. (2012). The Genesis of PGE Mineralization in the River Valley Intrusion, Ontario, Canada. Electronic Theses and Dissertations. University of Windsor, Earth and Environmental Sciences. 5600. http://scholar.uwindsor.ca/etd/5600.

Rollinson, H., Reid, C., & Windley, B. F. (2010). Chromitites from the Fiskenæsset anorthositic complex, West Greenland: clues to late Archaean mantle processes. In T. M. Kusky, M. Zhai, & W. Xiao (Eds.), *The Evolving Continents: Understanding Processes of Continental Growth* (Vol. 338, pp. 197–212), London: Geological Society of London, Special Publication.

Scoates, J. S. (2000). The plagioclase-magma density paradox re-examined and the crystallization of Proterozoic anorthosites. *Journal of Petrology, 41,* 627–649.

Şengör, A. M. C., & Natal'in, B. A. (2004). Phanerozoic analogues of Archaean oceanic basement fragments: Altaid ophiolites and ophirags. In T.M. Kusky (Ed.), *Precambrian Ophiolites and Related Rocks, Developments in Precambrian Geology* (Vol. 13, pp. 675–726) Elsevier, Amsterdam.

Shervais, J. W. (2003). Parent magmas of plutonic rocks in the Elder Creek Ophiolite, California; first approximation. Geological Society of America Annual Meeting, Colorado, Abstract 640.

Sleep, N., & Windley, B. F. (1982) Archean plate tectonics: constraints and inferences. *Journal of Geology, 90,* 363–379.

Steenfelt, A., Garde, A. A., Moyen, J. F. (2005). Mantle wedge involvement in the petrogenesis of Archaean grey gneisses in West Greenland. *Lithos, 79,* 207–228.

Stern, R. J. (2005). Evidence from ophiolites, blueschists, and ultrahigh-pressure metamorphic terranes that the modern episode of subduction tectonics began in Neoproterozoic time. *Geology, 33,* 557–560.

Stott, G. M. (1997). The Superior Province, Canada. In M. J. de Wit, & L. D. Ashwal (Eds.), Greenstone Belts (Vol. 35, pp. 480-507), Oxford: Oxford Monographs Geology and Geophysics.

Sun, S. S., & McDonough, W. F. (1989). Chemical and isotopic systematics of oceanic basalts: implications for mantle composition and processes. In A. D. Saunders, & M. J. Norry (Eds.), *Magmatism in the Ocean Basins* (Vol. 42, pp. 313-345), London: Geological Society of London, Special Publication.

Szilas, K., Hoffmann, J.E., Schulz T., Hansmeier, C., Polat, A., Viehmann, S., Kasper, H. U., & Münker, C. (2016). Combined bulk-rock Hf- and Nd-isotope compositions of Mesoarchaean metavolcanic rocks from the Ivisaartoq Supracrustal Belt, SW Greenland: Deviations from the mantle array caused by crustal recycling. *Chemie der Erde, 76,* 543–554.

Szilas, K., Van Hinsberg, V.J., Kisters, A. F. M., Hoffmann, J. E., Windley, B. F., Kokfelt, T. F., Scherstén, A., Frei, R., Rosing, M. T., & Münker, C. (2013). Remnants of arc-related Mesoarchean oceanic crust in the Tartoq Group of SW Greenland. *Gondwana Research, 23,* 436–451.

Szilas, K., Næraa, T., Scherstén, A., Stendal, H., Frei, R., van Hinsberg, V. J., Kokfelt, T. F., & Rosing, M. T. (2012). Origin of Mesoarchaean arc-related rocks with boninite/komatiite affinities from southern West Greenland. *Lithos, 144,* 24–39.

Takagi, D., Sato, H., & Nakagawa, M. (2005) Experimental study of low alkali tholeiite at 1-5 kbar: optimal condition for the crystallisation of high-An plagioclase in hydrous arc tholeiite. *Contributions to Mineralogy and Petrology, 149,* 527–540.

Windley, B. F., & Garde, A. A. (2009). Arc-generated blocks with crustal sections in the North Atlantic craton of West Greenland: new mechanism of crustal growth in the Archean with modern analogues. *Earth Science Reviews, 93,* 1–30.

Windley, B. F., Herd, R. K., & Bowden, A. A. (1973). The Fiskenæsset Complex, West Greenland, part 1; a preliminary study of the stratigraphy, petrology and whole-rock chemistry near Qeqertarssuatsiaq. Geological Survey of Greenland Bulletin, 106, p. 80, Copenhagen.

Windley, B. F., Smith, J. V. (1974). The Fiskenæsset Complex, West Greenland, part 2. General mineral chemistry from Qeqertarssuatsiaq. Grønlands Geologiske Undersøgelse Bulletin 108, p. 54, Copenhagen.

Wu, T., Polat, A., Frei, R., Fryer, B. J., Yang, K., & Kusky, T. (2016). Geochemistry, Nd, Pb and Sr Isotope Systematics, and U-Pb Zircon Ages of the Neoarchean Bad Vermilion Lake Greenstone Belt and Spatially Associated Granitic rocks, Western Superior Province, Canada. *Precambrian Research, 258,* 21-51.

Yang, X. M., Gilbert, H. P., & Houlé, M. G. (2012). Geological investigations of the Cat Creek area in the Neoarchean Bird River greenstone belt, southeastern Manitoba (part of NTS 52L12): new insights into PGE-Ni-Cu-Cr mineralization: Manitoba Innovation, Energy and Mines, Manitoba Geological Survey, Winnipeg, Report of Activities 2012, p. 32–53.

Yang, J., Shi, R., Wu, C., Su, D., & Chen, S. (2008). Petrology and SHRIMP age of Hongliugou Ophiolite at Milan, northern Altun on the northern margin of the Tibetan Plateau. *Acta Petrologica Sinica, 24,* 1567–1584.

Yurichev, A.N., & Chernyshov, A. I. (2014). Parental melt and geodynamics of the layered mafic-ultramafic massifs of the Kan block of Eastern Sayan. *Izvestiya Tomskogo Politekhnicheskogo Universiteta*, 1, 128-137.

Zhou, S., Polat, A., Longstaffe, F. J., Yang, K. G., Fryer, B. J., & Weisener, C. (2016). Formation of the Neoarchean Bad Vermilion Lake Anorthosite Complex and spatially associated granitic rocks at a convergent plate margin, Superior Province, Western Ontario, Canada. *Gondwana Research, 33,* 134-159.

Zirner, A., Ballhaus, C., Muenker, C., & Marien, C. (2013). Anorthosite dikes from Cyprus; phase relations in the system $CaAl_2Si_2O_8$ - $CaMgSi_2O_6$ - Mg_2SiO_4 at 5 Wt.% H_2O. Mineralogical Magazine, 77, p. 2621, Abstract.

Table and Figure Captions

Table 1. List of known anorthosite-bearing Phanerozoic ophiolites and their interpreted geodynamic setting.

Table 2. Major (wt.%) and trace element (ppm) compositions and significant element ratios of megacrystic plagioclase in leucogabbros at Sinarssuk, Fiskenæsset Complex.

Data Repository Table 1. Scanning Electron Microscope (SEM)-Energy Dispersive Spectroscopy (EDS) major element (wt.%) data and An content of plagioclase in leucogabbros and hornblendites in the Fiskenæsset Complex.

Figure 1. Simplified geological map of southern West Greenland showing the Meso-Neoarchaean crustal blocks of Ivittuut, Kvanefjord, Bjørnesund, Sermilik, Fiskefjord, and Maniitsoq (modified from Windley & Garde, 2009).

Figure 2. (a) Simplified tectonic map of the Superior Province (modified from Percival et al. 2012). A: Ashuanipi; B: Bienville; DH: Douglas Harbour; E: Eastmain; ERB: English River Belt; G: Goudalie; HBT: Hudson Bay Terrane; ILD: Island Lake Domain; KU: Kapuskasing Uplift; LG: La Grande; LM: Lac Minto; MRVT: Minnesota River Valley Terrane; MT: Marmion Terrane; NCT: North Caribou Terrane; O: Opatica; Op: Opinaca; OSD: Oxford-Stull Domain; PB: Pontiac Belt; Q: Qalluviartuuq; QB: Quetico Belt; T: Tikkerutuk; U: Utsalik; UD: Uchi Domain; WAT: Wawa-Abitibi Terrane; WRT: Winnipeg River Terrane; WWT: Western Wabigoon Terrane.

Figure 3. Field photographs of megacrystic leucogabbro and anorthosites in the Fiskenæsset Anorthosite Complex, western Greenland, showing the various stages of anorthosite development. Permanent marker has a length of 15 cm. (b) modified from Polat et al. (2009); (c) modified from Huang, Polat, Fryer, Appel, & Windley (2012).

Figure 4. Field photographs of leucogabbros, anorthosites, and differentiated sills in the Sinarssuk area of the Fiskenæsset Anorthosite Complex, West Greenland. (a) modified

from Polat et al. (2011); (b) and (d) modified from Polat et al. (2009); (c) and (f) modified from Huang et al. (2012).

Figure 5. Field photographs of anorthosites in the Ivisaartoq greenstone belt (a and b), and the Bad Vermilion Lake (c and d) and Doré Lake (e and f) anorthosite complexes. (e) modified from Polat, Frei, Longstaffe, & Woods (2017).

Figure 6. N-MORB-normalized trace element patterns for the Ivisaartoq (a) Fiskenasset (b), Bad Vermilion Lake (c), and Doré Lake (d) anorthosites. Data for (a), (b), (c) and (d) from Polat et al. (2008), Polat et al. (2009), Zhou et al. (2016), and Polat, Frei, Longstaffe, & Woods, (2017), respectively. Normalization values are from Sun & McDonough (1989).

Figure 7. Simplified geodynamic model for the origin of Archaean anorthosite-bearing layered intrusions (modified from Polat et al., 2008). (c) shows an example of mineralogically stratified sill, representing a small version of Archaean magma chambers.

Figure 8. Field photographs of plagioclase megacrysts in the Fiskenæsset Complex. Dark to grey cores are relict igneous plagioclase, whereas clear to white rims and patches represent the recrystallized metamorphic plagioclase. (b) modified from Huang, Fryer, Polat, & Pan (2014); (d) modified from Polat et al. (2009).

Figure 9. Photomicrographs across two megacrystic plagioclase grains, illustrating the preservation of igneous plagioclase in the Fiskenæsset Complex despite deformation and metamorphism. Optical continuity (e.g., albite twinning) in igneous plagioclase grains suggests that they formed as 6-8 cm long single crystal in a magma chamber. Albite twins in large igneous crystals are overprinted by smaller metamorphic crystals.

Figure 1

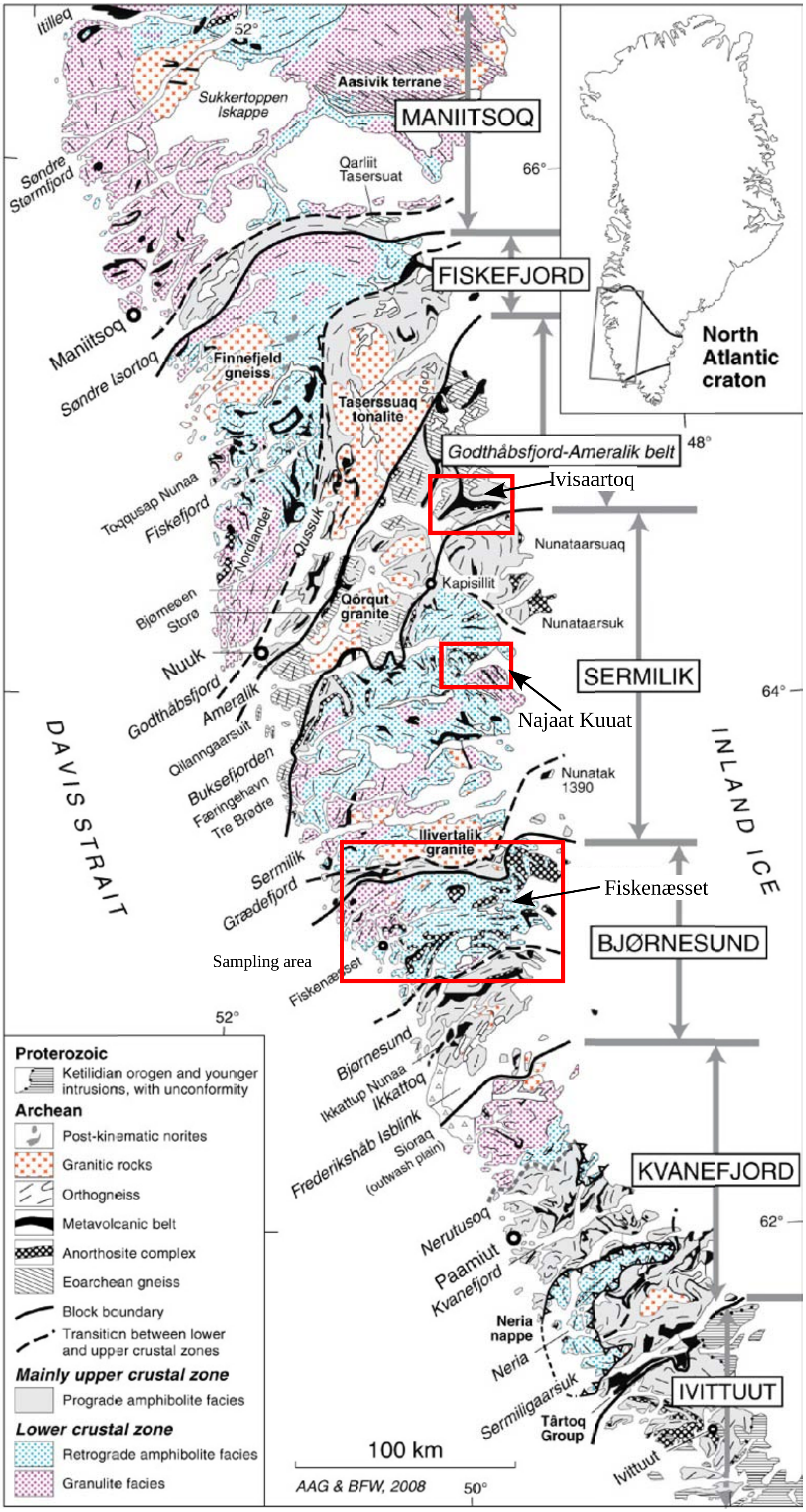
MANIITSOQ
FISKEFJORD
Godthåbsfjord-Ameralik belt
Ivisaartoq
SERMILIK
Najaat Kuuat
Fiskenæsset
Sampling area
BJØRNESUND
KVANEFJORD
IVITTUUT
North Atlantic craton
DAVIS STRAIT
INLAND ICE
Aasivik terrane
Sukkertoppen Iskappe
Qarliit Tasersuat
Søndre Strømfjord
Itilleq
Maniitsoq
Søndre Isortoq
Finnefjeld gneiss
Taserssuaq tonalite
Toqqusap Nunaa
Fiskefjord
Nordlandet
Qussuk
Nunataarsuaq
Kapisillit
Qôrqut granite
Nunataarsuk
Bjørneøen
Storø
Nuuk
Godthåbsfjord
Ameralik
Qilanngaarsuit
Buksefjorden
Færingehavn
Tre Brødre
Nunatak 1390
Ilivertalik granite
Sermilik
Grædefjord
Fiskenæsset
Bjørnesund
Ikkattup Nunaa
Ikkattoq
Frederikshåb Isblink
Sioraq (outwash plain)
Nerutusoq
Paamiut
Kvanefjord
Neria nappe
Neria
Sermiligaarsuk
Tårtoq Group
Ivittuut
52°
66°
48°
64°
62°
50°
100 km
AAG & BFW, 2008
Proterozoic
Ketilidian orogen and younger intrusions, with unconformity
Archean
Post-kinematic norites
Granitic rocks
Orthogneiss
Metavolcanic belt
Anorthosite complex
Eoarchean gneiss
Block boundary
Transition between lower and upper crustal zones
Mainly upper crustal zone
Prograde amphibolite facies
Lower crustal zone
Retrograde amphibolite facies
Granulite facies

Figure 2 Click here to download Figure Figure 2.pdf

Figure 2

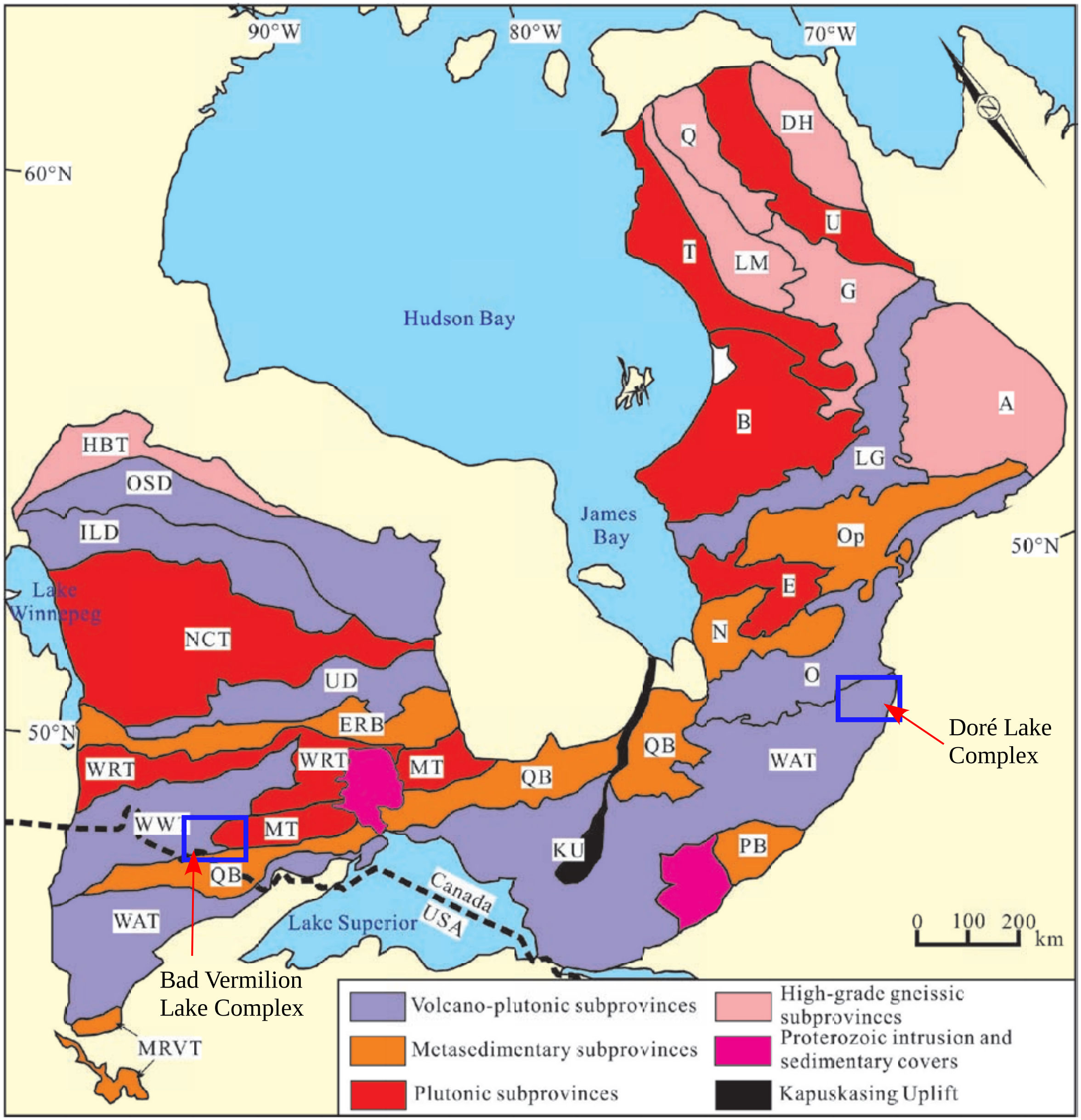

Figure 3

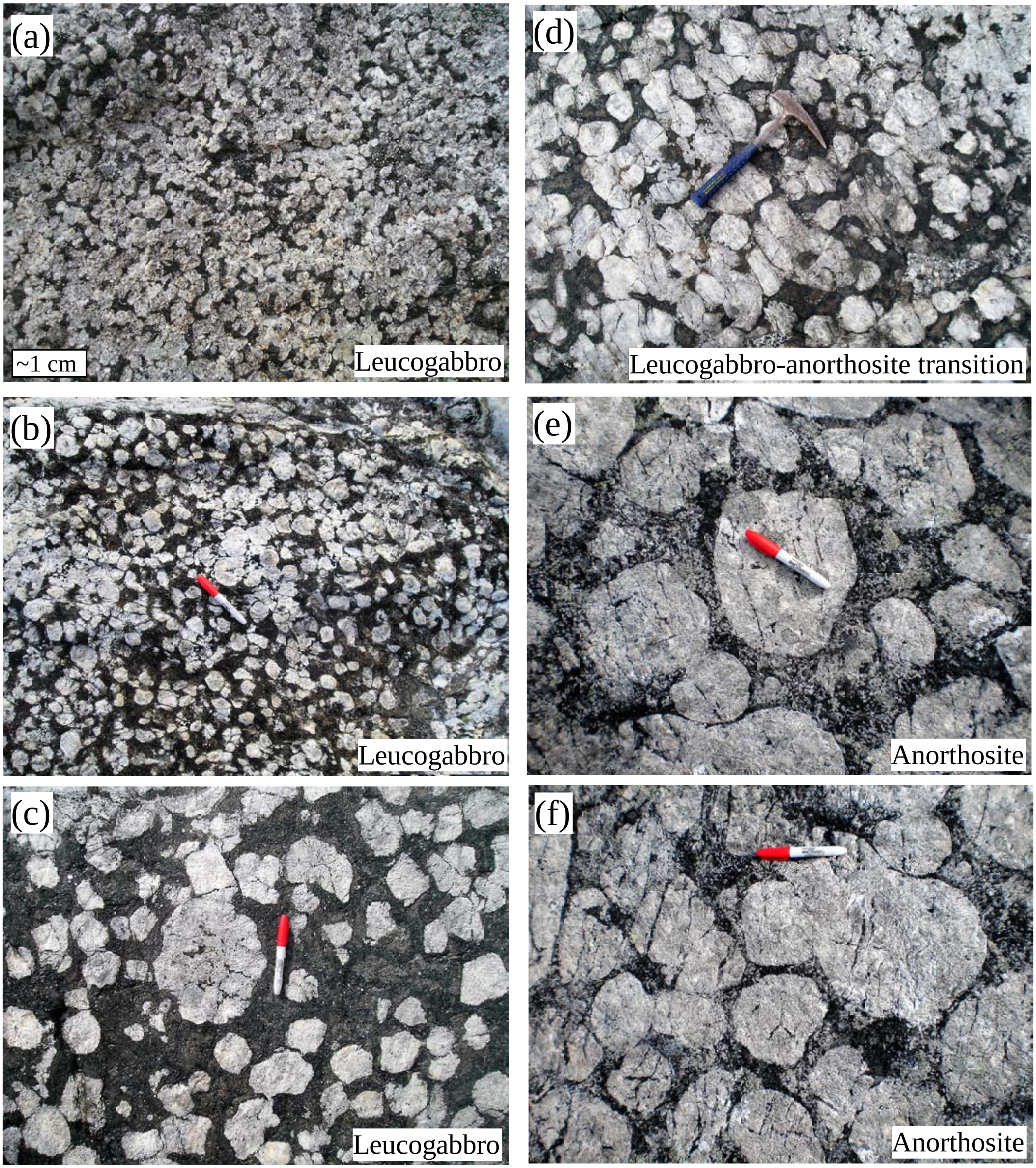
(a)
~1 cm
Leucogabbro
(d)
Leucogabbro-anorthosite transition
(b)
Leucogabbro
(e)
Anorthosite
(c)
Leucogabbro
(f)
Anorthosite

Figure 4

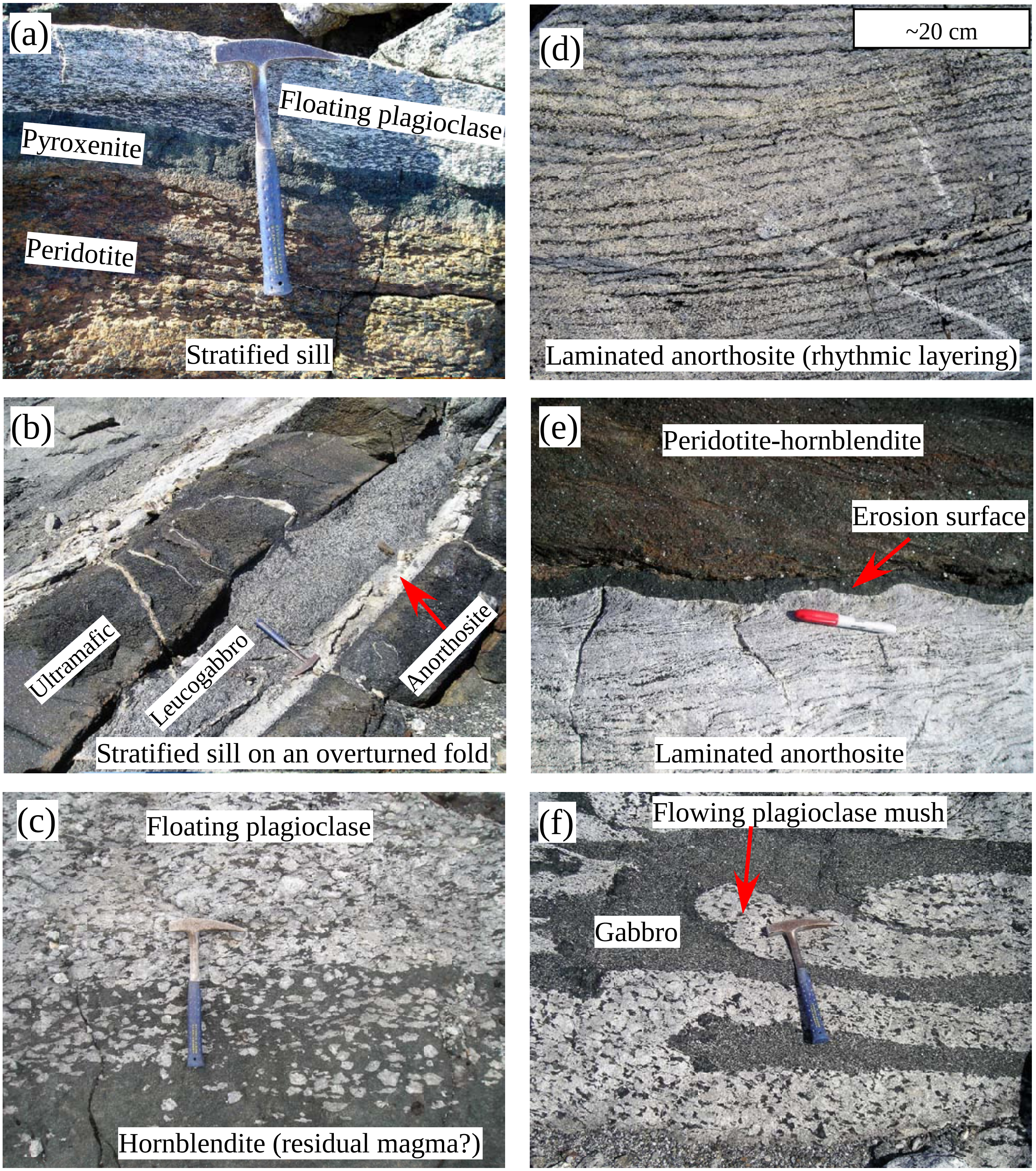
(a)
Floating plagioclase
Pyroxenite
Peridotite
Stratified sill
(d)
~20 cm
Laminated anorthosite (rhythmic layering)
(b)
Ultramafic
Leucogabbro
Anorthosite
Stratified sill on an overturned fold
(e)
Peridotite-hornblendite
Erosion surface
Laminated anorthosite
(c)
Floating plagioclase
Hornblendite (residual magma?)
(f)
Flowing plagioclase mush
Gabbro

Figure 5

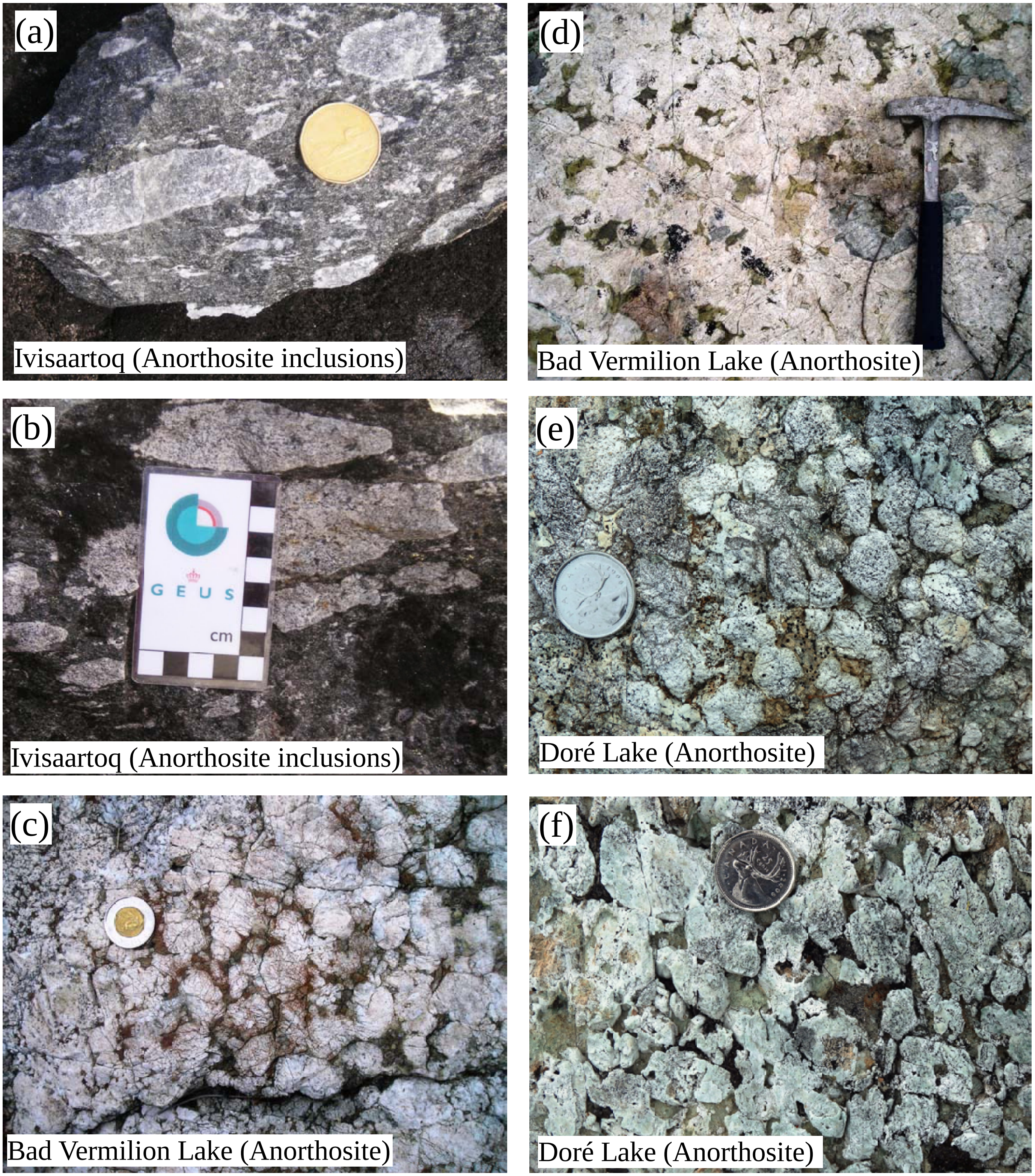
(a)
Ivisaartoq (Anorthosite inclusions)
(d)
Bad Vermilion Lake (Anorthosite)
(b)
GEUS
cm
Ivisaartoq (Anorthosite inclusions)
(e)
Doré Lake (Anorthosite)
(c)
Bad Vermilion Lake (Anorthosite)
(f)
Doré Lake (Anorthosite)

Figure 6

Click here to download Figure Figure 6.docx

Figure 6

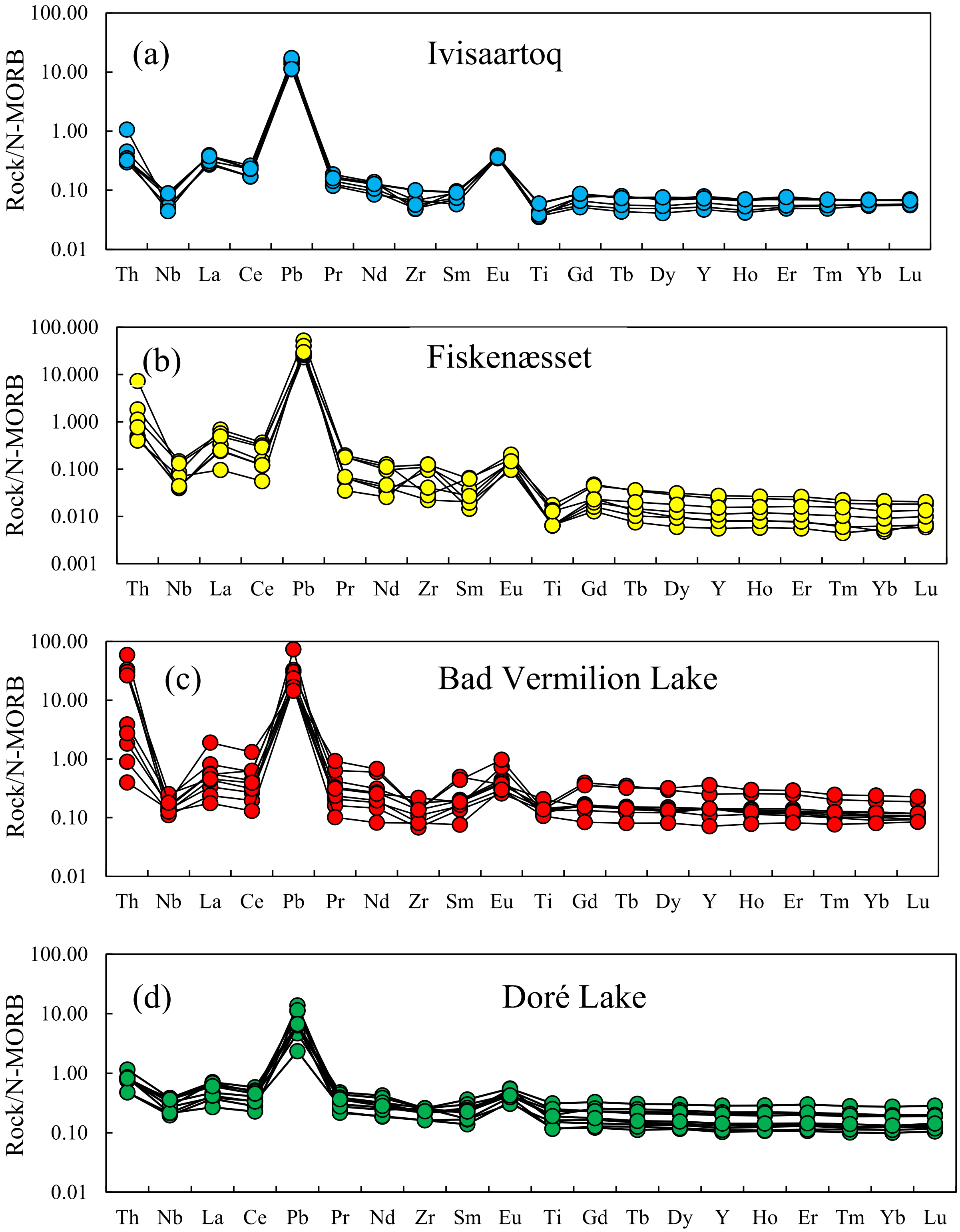

Figure 7

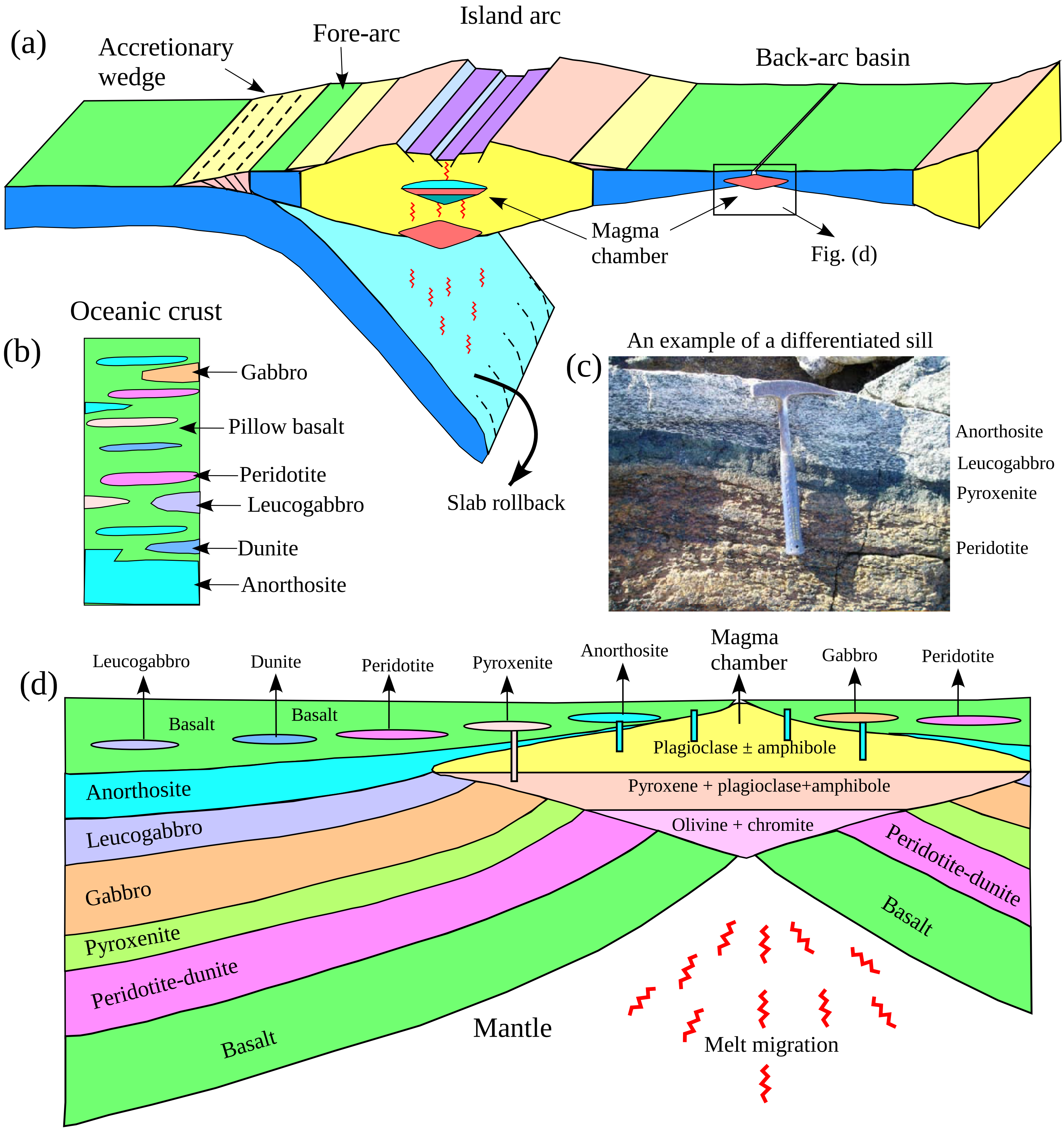
(a)
Accretionary wedge
Fore-arc
Island arc
Back-arc basin
Magma chamber
Fig. (d)
Slab rollback
(b)
Oceanic crust
Gabbro
Pillow basalt
Peridotite
Leucogabbro
Dunite
Anorthosite
(c)
An example of a differentiated sill
Anorthosite
Leucogabbro
Pyroxenite
Peridotite
(d)
Leucogabbro
Dunite
Peridotite
Pyroxenite
Anorthosite
Magma chamber
Gabbro
Peridotite
Basalt
Basalt
Plagioclase ± amphibole
Pyroxene + plagioclase+amphibole
Olivine + chromite
Anorthosite
Leucogabbro
Gabbro
Pyroxenite
Peridotite-dunite
Basalt
Mantle
Peridotite-dunite
Basalt
Melt migration

Figure 8

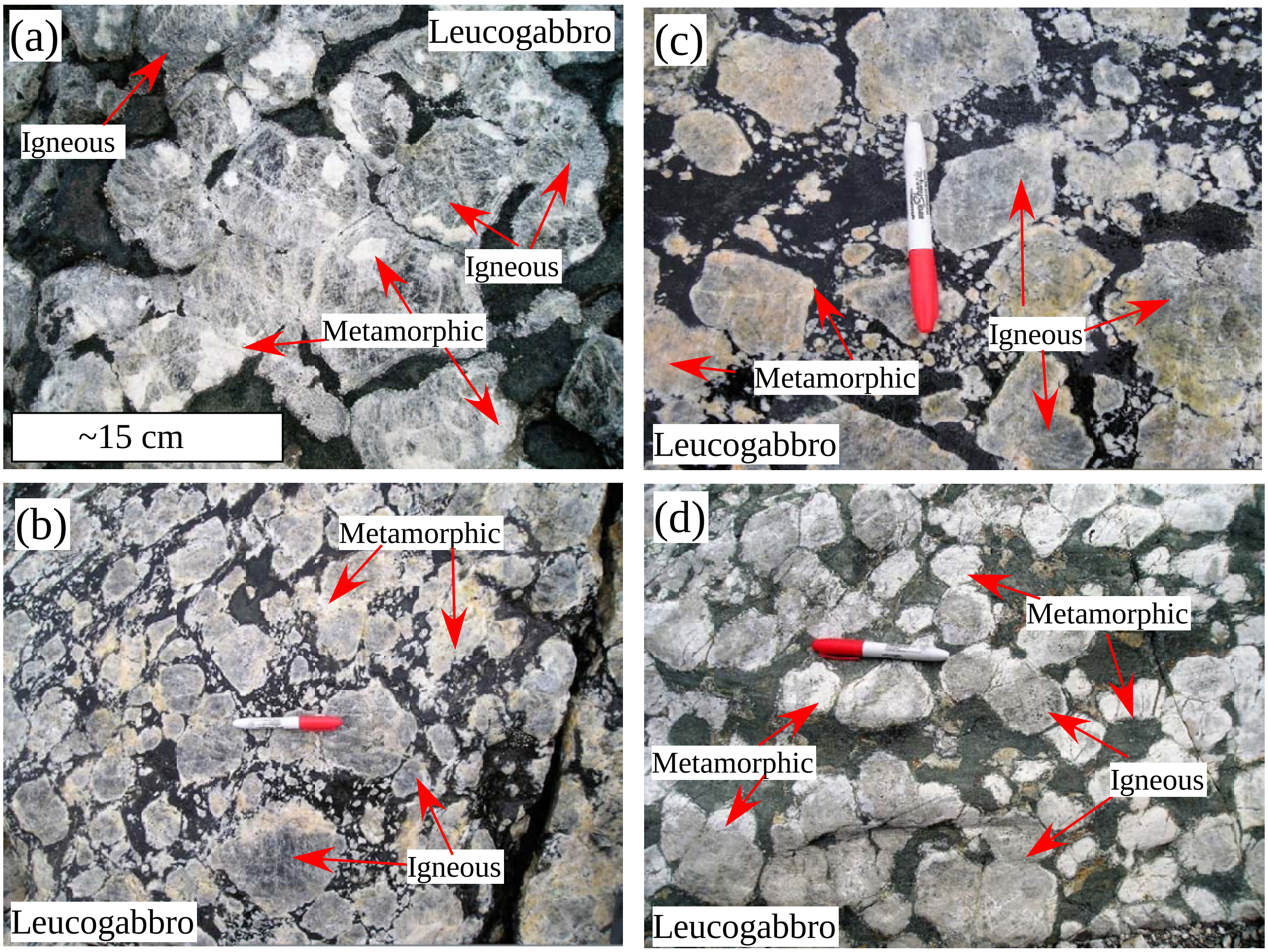
(a)
Leucogabbro
Igneous
Igneous
Metamorphic
~15 cm
(c)
Igneous
Metamorphic
Leucogabbro
(b)
Metamorphic
Igneous
Leucogabbro
(d)
Metamorphic
Metamorphic
Igneous
Leucogabbro

Figure 9

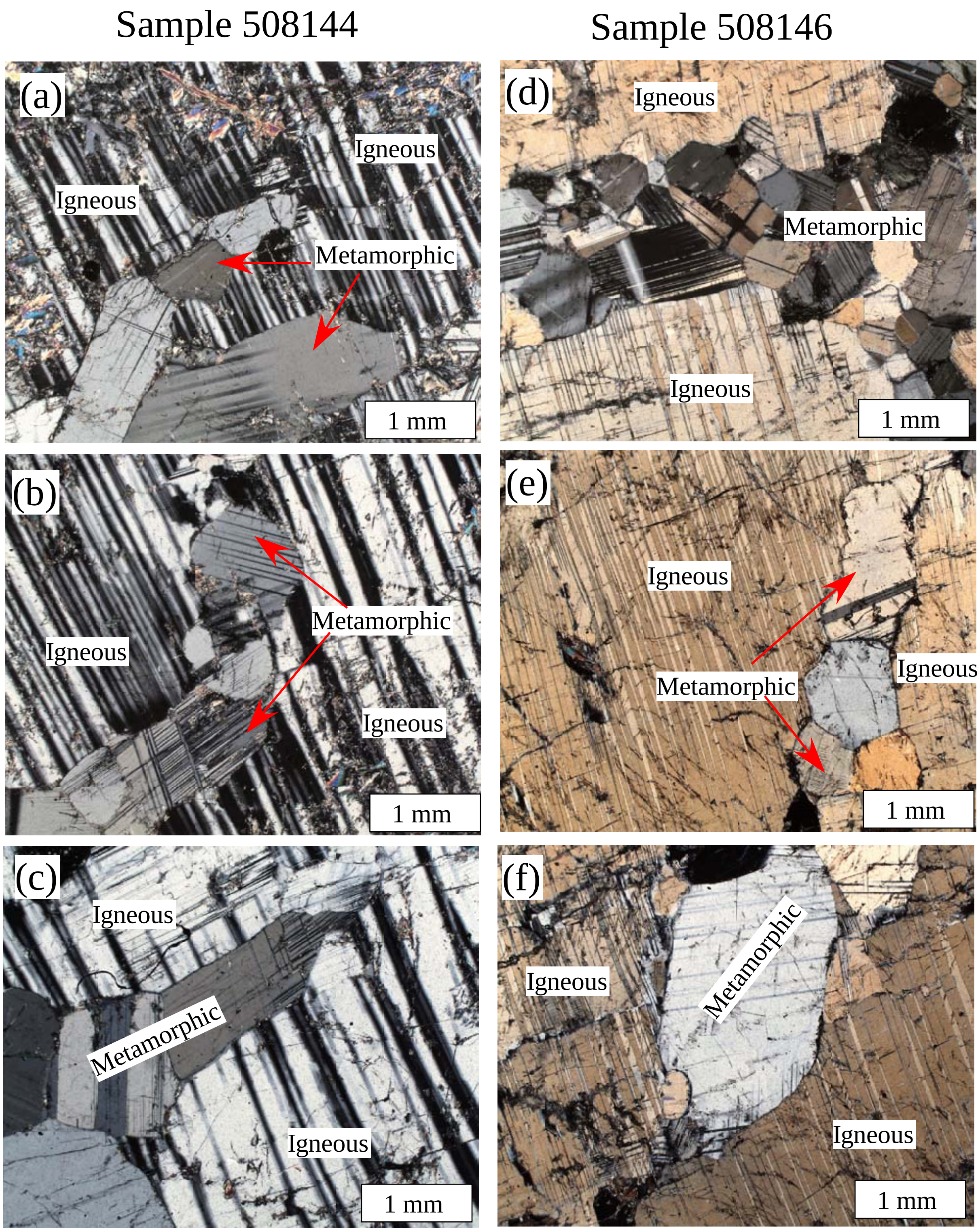
Sample 508144
Sample 508146
(a)
Igneous
Igneous
Metamorphic
1 mm
(d)
Igneous
Metamorphic
Igneous
1 mm
(b)
Metamorphic
Igneous
Igneous
1 mm
(e)
Igneous
Igneous
Metamorphic
1 mm
(c)
Igneous
Metamorphic
Igneous
1 mm
(f)
Igneous
Metamorphic
Igneous
1 mm

Table 1 Click here to download Table Table 1.pdf

Table 1. List of known anorthosite-bearing Phanerozoic ophiolites and their interpreted geodynamic setting.

Ophiolite	Age	Interpreted geodynamic setting	References
Camaguey Ophiolite, Cuba	Jurassic	Suprasubduction zone	Henares et al. (2010)
Mazhalyk Ophiolite, Russia	Ordovician	Suprasubduction zone, island arc	Borodina et al. (2004)
Zambales Ophiolite, the Philippines	Eocene	Suprasubduction zone	Hawkins (2007)
Talazhinskiy Ophiolite, Russia	Paleozoic?	Suprasubduction zone	Yurichev and Chernyshov (2014)
Chilas Complex, Pakistan	Jurassic - Cretaceous	Suprasubduction zone, island arc	Khan et al. (1989)
Bay of Islands Ophiolite, Nefoundland (Canada)	Ordovician	Suprasubduction zone	Komor and Elthon (1990)
Zhaheba Ophiolite, China	Cambrian-Ordovician	Suprasubduction zone	Jian et al. (2003)
Halifax County Complex, North Carolina (USA)	Early Paleozoic	Suprasubduction zone, island arc	Kite and Stoddard (1984)
Troodos Ophiolite, Cyprus	Cretaceous	Suprasubduction zone, backarc basin	Zirner et al. 2013
Urmia Ophiolite, Iran	Devonian	Suprasubduction zone, island arc	Fazlnia and Alizade (2013)
Solonker Ophiolite, China and Mongolia	Permian-Triassic	Mid ridge to island arc	Jian et al. (2010)
Kahnuj Ophiolite, Iran	Jurassic-Cretaceous	Mid ocean ridge	Arvin et al. (2005)
Mariana Arc, the Philippines	Cenozoic	Suprasubduction zone, backarc basin	Newman et al. (2000), Hawkins (2007)
Buck Creek Ophiolite, North Caroline (USA)	Paleozoic	Suprasubduction zone	Peterson et al. (2009)
Karayasmak Alaskan-type intrusion, Turkey	Carboniferous	Suprasubduction zone	Eyuboglu et al. (2010)
Hongliugou Ophiolite, China	Cambrian-Ordovician	Suprasubduction zone	Yang et al. (2008)
Lizard Ophiolite, England	Devonian	Suprasubduction zone	Leake and Styles (1984)
Oman Ophiolite, Oman	Cretaceous	Suprasubduction zone	Boudier and Nicolas (2011a, 2011b)
Jinshajjiang Ophiolite, China	Carboniferous?	Unkonwn	Jian et al. (1999)
Leka Ophiolite, Norway	Cambrian-Ordovician	Unkonwn	Austrheim and Prestvik (2008)
Othrys Ophiolite, Greece	Mesozoic	Suprasubduction zone?	Mitsis and Economou-Eliopoulos (2001)
East Sulawesi Ophiolite, Indenosia	Cenozoic	Suprasubduction zonbe, mid ocean ridge	Partkinson (1998); Kadarusman et al. (2004)
Elder Creek Ophiolite, California (USA)	Mesozoic	Suprasubduction zone, forearc	Shervais (2003)

Table 2. Major (wt.%) and trace element (ppm) compositions and significant element ratios of megacrystic plagioclase in leucogabbros at Sinarssuk, Fiskenæsset Complex

	508142	508144	508146	508148	508154	508156	508161	Averge (n=7)
SiO_2	47.72	46.90	46.71	47.68	48.72	48.22	47.09	47.58
TiO_2	0.01	0.01	0.01	0.01	0.02	0.02	0.02	0.01
Al_2O_3	32.76	32.99	33.51	33.22	31.90	32.35	32.86	32.80
Fe_2O_3	0.48	0.90	0.52	0.53	0.83	0.80	1.10	0.74
MnO	0.02	0.01	0.02	0.02	0.01	0.01	0.02	0.02
MgO	0.18	0.30	0.22	0.31	0.30	0.22	0.33	0.27
CaO	15.34	16.14	16.77	14.94	15.31	15.79	16.22	15.79
K_2O	1.81	0.97	0.48	1.48	0.33	0.28	0.40	0.82
Na_2O	1.65	1.75	1.77	1.80	2.55	2.28	1.96	1.97
P_2O_5	0.01	0.03	0.01	0.01	0.03	0.02	0.01	0.02
LOI	2.64	1.77	1.13	1.66	0.99	0.97	0.74	1.41
Mg-number (%)	43	40	46	53	42	36	37	42
An-content (%)	82	86	86	82	78	80	85	83
Co	2	2	2	2	3	2	3	2
Rb	63	38	18	54	10	10	12	29
Sr	165	145	112	172	143	177	122	148
Cs	0.44	0.52	0.14	0.79	0.12	0.13	0.09	0.32
Ba	232	115	51	307	45	41	65	122
V		8.1		5.1	7.1	5.0	7.1	6.5
Ta	0.018	0.007	0.015	0.018	0.034	0.035	0.012	0.02
Nb	0.201	0.092	0.100	0.162	0.342	0.310	0.102	0.19
Zr	8.15	7.13	1.64	9.35	2.07	9.23	3.02	5.80
Hf	0.189		0.038	0.208	0.063	0.235	0.053	0.13
Th	0.881	0.059	0.055	0.048	0.221	0.134	0.093	0.21
U	0.446	0.018	0.023	0.097	0.113	0.085	0.071	0.12
Y	0.23	0.16	0.22	0.31	0.67	0.77	0.43	0.40
La	1.712	0.827	0.604	0.240	1.428	1.223	0.625	0.95
Ce	2.722	1.118	0.903	0.417	2.382	2.198	0.911	1.52
Pr	0.238	0.086	0.084	0.046	0.257	0.236	0.091	0.15
Nd	0.706	0.252	0.297	0.187	0.922	0.812	0.339	0.50
Sm	0.097	0.038	0.053	0.052	0.172	0.163	0.071	0.09
Eu	0.140	0.116	0.145	0.098	0.164	0.208	0.149	0.15
Gd	0.087	0.047	0.059	0.073	0.173	0.164	0.084	0.10
Tb	0.009	0.005	0.007	0.010	0.023	0.024	0.014	0.01
Dy	0.044	0.027	0.042	0.056	0.128	0.141	0.081	0.07
Ho	0.008	0.006	0.008	0.012	0.024	0.027	0.016	0.01
Er	0.022	0.017	0.023	0.033	0.066	0.077	0.048	0.04
Tm	0.003	0.002	0.003	0.005	0.009	0.010	0.007	0.01
Yb	0.015	0.016	0.019	0.028	0.055	0.065	0.039	0.03
Lu	0.003	0.003	0.003	0.005	0.008	0.009	0.006	0.01
Cu	6.0			19.9	4.9	8.5	8.0	9.45
Ga	87	64	50	108	47	49	51	65
Pb	15.7	7.0	8.0	12.1	8.1	8.6	8.9	9.8
Li	19.9	14.0	14.4	19.3	13.5	11.5	12.9	15.1
La/Sm_{cn}	11.41	13.91	7.31	3.00	5.35	4.83	5.66	7.35
La/Yb_{cn}	83.7	36.2	22.8	6.2	18.6	13.6	11.5	27.5
Gd/Yb_{cn}	4.92	2.39	2.59	2.17	2.60	2.10	1.79	2.65
Eu/Eu*	4.66	8.30	7.88	4.91	2.91	3.88	5.88	5.49
Ce/Ce*	1.05	1.03	0.98	0.97	0.96	1.00	0.94	0.99
Pb/Pb*	327	591	845	3741	186	222	900	462
Al_2O_3/TiO_2	3988	3994	4144	4046	1438	1883	2019	3073
Nb/Nb*	0.06	0.15	0.20	0.55	0.22	0.28	0.15	0.23
Zr/Zr*	2.18	5.05	0.91	6.65	0.36	1.77	1.36	2.61
Ti/Ti*	0.13	0.20	0.17	0.17	0.26	0.20	0.29	0.20
North	63° 21' 24.2"	63° 21' 24.2"	63° 21' 22.6"	63° 21' 21.4"	63° 20' 56.7"	63° 20' 56.7"	63° 21' 06.2"	
West	49° 16' 42.3"	49° 16' 42.3"	49° 16' 42.5"	49° 16' 41.8"	49° 16' 17.2"	49° 16' 17.2"	49° 16' 28.7"	

Supplementary Data Table 1. Scanning Electron Microscope (SEM)-Energy Dispersive Spectroscopy (EDS) major element (wt.%) data and anorthite (An%) content of plagioclase in leucogabbros and hornblendites in the Fiskenæsset Complex

Sample#	509193 (Leucogabbro)							
Spot#	1	2	3	4	5	6	7	8
Na_2O	2.1	3.2	2.3	2.3	1.6	2.5	2.3	3.0
Al_2O_3	33.9	31.7	33.8	33.4	34.7	33.3	33.2	32.2
SiO_2	49.2	51.9	49.7	49.6	48.1	49.8	50.0	51.3
CaO	14.8	13.1	14.2	14.7	15.7	14.4	14.5	13.5
Total	100.0	100.0	100.0	100.0	100.0	100.0	100.0	100.0
An (%)	76	66	75	75	81	74	74	68

Sample#	509092 (Leucogabbro)					
Spot#	1	2	3	4	5	6
Na_2O	2.3	1.6	1.7	1.9	1.9	1.6
Al_2O_3	33.7	34.7	35.0	34.1	34.2	34.7
SiO_2	49.0	48.0	47.9	48.7	48.2	48.0
CaO	15.0	15.7	15.4	15.4	15.8	15.7
Total	100.0	100.0	100.0	100.0	100.0	100.0
An%	77	81	82	79	80	81

Sample#	509103 (Hornblendite)										
Spot#	1	2	3	4	5	6	7	8	9	10	11
Na_2O	1.11	1.04	1.08	0.99	0.89	0.97	1.04	1.12	0.93	1.00	1.07
Al_2O_3	36.76	36.62	36.91	37.12	36.67	36.65	36.5	36.84	36.3	36.42	36.76
SiO_2	45.54	45.62	45.24	45.09	45.84	45.67	45.56	45.79	47.26	45.64	45.62
CaO	16.59	16.71	16.77	16.79	16.6	16.71	16.9	16.24	15.51	16.95	16.55
Total	100	100	100	100	100	100	100	100	100	100	100
An (%)	92	93	90	90	90	90	91	90	90	90	91